

# Properties of high pressure phases in metal-hydrogen systems

E. G. Ponyatovskii, V. E. Antonov, and I. T. Belash

*Institute of Solid State Physics, Academy of Sciences of the USSR, Chernogolovka (Moscow Oblast')*  
Usp. Fiz. Nauk 137, 663-705 (August 1982)

The development of high-pressure technology has in recent years permitted obtaining extensive new information on the properties of hydrides of group VI-VIII transition metals. In this review, the experimental procedures for compressing macroscopic quantities of hydrogen to record high pressures, phase transitions, and structures of new high-pressure phases in Me-H systems are briefly described. Special attention is devoted to the magnetic properties of solid solutions of hydrogen in 3d metals and their alloys, whose study has yielded definite conclusions concerning the effect of hydrogen on the band structure and exchange interaction in these materials. The role of structural instabilities in the formation of superconducting properties of hydrogen solutions in 4d metal alloys based on palladium is examined.

PACS numbers: 74.70.Lp, 75.30.Et, 64.70.Kb, 62.50. + p

## CONTENTS

1. Introduction	596
2. Method for compressing hydrogen and obtaining hydrides	597
3. Phase equilibria in metal-hydrogen systems	599
4. Magnetic properties of metal-hydrogen solutions	603
a) Magnetic properties of Ni-Me alloys. b) Ni-Me-H solutions. 1) Ni-Fe-H system, 2) Ni-Co-H system, 3) Ni-Mn-H system, 4) Ni-Cr-H system, 5) Discussion of the properties of Ni-Me-H solutions. c) $Fe_{65}(Ni_{1-x}Mn_x)_{35}$ -H solutions. d) Applicability of the rigid d-band model for describing magnetic properties of other Me-H solutions. 1) Hydrogen solutions in fcc alloys based on 3d metals, 2) Solutions of hydrogen in 3d metals with hcp lattice, 3) Solutions in hydrogen in fcc alloys of 4d metals, 4) Ni-Fe-C solutions.	
5. Superconductivity of hydrogen solutions in palladium alloys	615
6. Conclusions	618
References	618

## 1. INTRODUCTION

The properties of transition metal-hydrogen systems draw the close attention of researchers working in the most diverse areas of physics and physical materials technology. There are many reasons for the continuously increasing interest in the problem of hydrogen in metals, including the increasing use of metal-hydrogen systems in practice (absorption of nuclear radiation, storage of hydrogen and hydrides, purification of hydrogen, hydrogen isotope separation development of new types of heat exchangers, catalyzers, and so on) and by the very strong influence of hydrogen dissolved even in small quantities on structural materials (hydrogen brittleness, corrosion in acidic media, erosion of materials in contact with hydrogen plasma, etc.).

Metal-hydrogen systems have a number of unique physical properties and have already served for a long time as convenient model objects for studying a wide range of physical phenomena in solids. Thus, for example, the Pd-H system was the first and still remains the classical example of so-called nonstoichiometric compounds.<sup>1</sup> The theory of nonideal solutions of hydrogen in palladium proposed by Lacher<sup>2</sup> anticipated the creation of the concept of a three dimensional lattice gas<sup>3</sup>; the behavior of the Pd-H system near the "lattice gas-lattice liquid" critical point is an excellent example

of all the basic assumptions of the theory of second-order phase transitions proposed by Landau<sup>4</sup> being satisfied. Due to the extremely high mobility of hydrogen in metals, restructuring of the hydrogen sublattice in metal-hydrogen systems can occur at very low temperatures, which makes these systems convenient model objects for experimental study of ordering phenomena in solids as well. This problem is examined in detail in Ref. 5. There is an extensive literature on the possibility of very nontrivial phenomena in metal-hydrogen systems, such as, for example, quantum diffusion and high-temperature superconductivity, resulting from the characteristic quantum behavior of hydrogen in a metallic matrix. Refs. 6-9 give a detailed introduction to these problems.

All these unusual properties of metal-hydrogen systems are related to the properties of hydrogen as one of the components of these systems, primarily its extremely low mass and absence of filled electron shells: the  $H^+$  ion is simply a proton. For this reason, the key to understanding the entire complex of physical properties of such systems is the problem of the physical status of hydrogen in transition metals. In recent years, there has been appreciable progress along these lines. Interesting work on calculation of the band structures of hydrides has been performed by Switen-

dick,<sup>10</sup> Papaconstantopolous *et al.*,<sup>11,12</sup> Gupta,<sup>13</sup> Kulkov,<sup>14</sup> and others. However, further development of the theory is limited by the scarcity of experimental data on the structure and physical properties of transition metal-hydrogen systems. The basic experimental results for solutions with a relatively high hydrogen content (>1 at.%) were obtained for group IV and V metals (Ti, Zr, Hf, V, Nb, Ta) and palladium. As is well known, 14 of 15 transition metals in groups VI–VIII, including such important and interesting metals as Fe, Co, Ni, Cr, Mn, and Mo, do not form hydrides under equilibrium conditions at hydrogen pressures of the order of atmospheric pressure. The enormous amount of experimental information on the influence of hydrogen on the properties of these metals and alloys based on them was obtained for hydrogen concentrations usually not exceeding  $10^{-3}$ – $10^{-5}$  at.%,<sup>15-17</sup> comparable to the total concentration of various defects, hydrogen traps, which makes it difficult to give a correct physical interpretation of these data.

Work on the development of methods for saturating metals with hydrogen under nonequilibrium conditions (electrochemical and plasma methods, hydrogen implantation) was begun a long time ago and continues successfully. For example, electrochemical methods first permitted obtaining chromium<sup>18</sup> and nickel<sup>19</sup> hydrides, implantation methods permitted obtaining molybdenum dideuteride<sup>20</sup> and superstoichiometric palladium hydride PdH<sub>1.33</sub> with a tetragonal lattice that is unusual for transition metal hydrides.<sup>21</sup> But, under nonequilibrium conditions it is difficult and in many cases practically impossible to obtain sufficiently homogeneous specimens and to vary in a controlled manner the content of hydrogen in them. Moreover, it is far from always possible to be sure that the physical properties of specimens obtained by such methods will be close to equilibrium.

There is a direct way to avoid all these difficulties: to synthesize hydrides by placing metals in a hydrogen atmosphere, whose thermodynamic potential is increased by compression to high pressures. However, work with high-pressure gases involves many experimental difficulties and even for inert gases the upper limit of pressures attainable with the help of more or less assimilated techniques does not exceed 20–30 kbar. In the case of hydrogen, these difficulties are considerably increased by its high compressibility, extremely low viscosity, and chemical corrosiveness, which greatly increase with pressure and temperature. For this reason, up to the last decade, the study of metal-hydrogen systems was limited by pneumatic pressures (100–150 bar) and in individual cases by pressures up to several kbar.

In recent years, there has been a qualitative jump in the development of nontraditional methods for compressing gaseous hydrogen, which permitted obtaining a large quantity of new experimental data on metal-hydrogen systems, the generalization and discussion of which is the subject of the present review. Special attention will be devoted to the magnetic properties of hydrogen solutions in 3d metal alloys, whose study

permitted making a number of definite conclusions concerning the effect of hydrogen on the band structure and exchange interaction in transition metals. We shall also briefly describe new methods for compressing hydrogen in macroscopic volumes to pressures of tens of kilobars, with which we shall begin the review.

## 2. METHODS FOR COMPRESSING HYDROGEN AND OBTAINING HYDRIDES

The mechanical properties of existing structural materials, not subjected to hydrogen brittleness (primarily beryllium bronze) permit compressing hydrogen to pressures of 5–12 kbar. This range of pressures was first exceeded in the middle of the 1960s by Polish scientists who developed a system in which compressed hydrogen was isolated from the walls of the high-pressure chamber, which permitted using steel chambers.<sup>22,23</sup> For this purpose, an ampoule, made of material impermeable to hydrogen, was placed with the closed end upwards into the working channel of a piston-cylinder type chamber, the chamber was filled with kerosene, and a preliminary pressure of 120–150 bar was created in it. Hydrogen was introduced from an external source through a special system of seals, channels, and valves into the ampoule at a somewhat higher pressure. Then the injection system was cut off from the working volume of the chamber and the pressure could be increased further in the hydrogen bubble formed, by compressing the pressure transmitting medium (kerosene) as in an ordinary hydrostatic chamber. The hydrogen-filled ampoule is subjected only to hydrostatic pressure, which minimizes the required mechanical strength; in Refs. 22 and 23, it was made of copper. In chambers with the construction described here, the hydrogen could be compressed to pressures ~15 kbar at temperatures close to room temperature.

The next step in extending the working hydrogen pressure range consisted of eliminating injection of hydrogen into the ampoule directly in the high-pressure chamber (the presence of the corresponding system of channels and seals greatly decreased the strength properties of the chamber). Hydrogen was compressed in a special container placed in an ordinary hydrostatic chamber.<sup>23,24</sup> The hydrogen was first pumped into a container at a pressure of 0.2–0.5 kbar with the help of a special compressor. The container consisted of beryllium bronze and was equipped with a system of gas seals, capable of withstanding this preliminary pressure. One of the variants of such a system consisting of two piston-cylinder systems (I and II) placed one inside the other is shown in Fig. 1. All the empty space within system I was filled with kerosene. At room temperature, such systems permitted compressing hydrogen to pressures of 25–30 kbar,<sup>23,24</sup> and up to ~13 kbar up to 450 °C<sup>25</sup> (in the latter case, a miniature heater was placed inside system II). The significant widening of the pressure and temperature ranges made it possible to synthesize nickel and chromium hydrides under equilibrium conditions and to obtain for the first time manganese hydride and hydrogen saturated phases based on an entire series of nickel and palladium al-

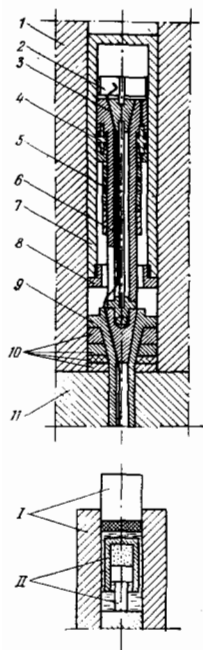


FIG. 1. Diagram of the apparatus for compressing hydrogen.<sup>23</sup>

1) High pressure chamber of the first piston-cylinder system; 2) specimen and auxiliary apparatus; 3) socket for the electrical input to the second piston-cylinder system; 4) packing; 5) spring; 6) electrical input leads (12–14 wires); 7) hydrogen container cylinder; 8) nut; 9) socket for electrical input to the first piston-cylinder system; 10) liners for the electrical input socket; 11) foundation of the high-pressure chamber.

loys, to study their crystalline structure and thermal stability, and to begin studying magnetic and superconducting properties (a detailed review of work performed during this period is given in Refs. 26 and 27).

Pressures of the order of 30 kbar practically exhaust the possibilities of hydrostatic piston-cylinder type chambers. We were able to overcome this barrier by using the method proposed in Ref. 28 for obtaining high-pressure hydrogen. The method consisted of the following. A condensed hydrogen-containing compound is introduced into an ampoule type container. The container is placed into the high-pressure chamber, preliminary compression is performed, and the hydrogen is freed by decomposing the compound by any known method [for example, by heating (thermal decomposition), by an electrical current (electrolysis), by performing an exchange chemical reaction to liberating hydrogen]. Then the temperature and pressure in the working zone of the high pressure chamber and, therefore, of the hydrogen in the container as well, are brought up to the necessary values. Based on this method, a series of high-pressure cells was created at the Institute of Solid State Physics of the USSR Academy of Sciences, which permit studying the behavior of the Curie points and electrical resistance of specimens in a range of hydrogen pressures from 0.03 to 70 kbar at  $-150 \leq T \leq 500^\circ\text{C}$ .

The simplest method for liberating hydrogen from the compound is thermal decomposition. Diagrams of cells for measuring the electrical resistance of specimens in

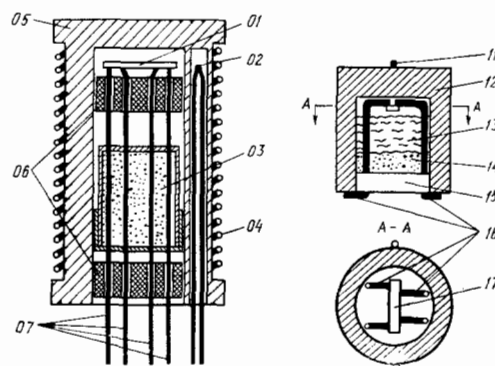


FIG. 2. Diagram of cells for measuring the electrical resistance of specimens in a hydrogen atmosphere using hydrostatic (01–07) and quasihydrostatic (11–17) high-pressure chambers.

01, 17) specimens; 02, 11) thermocouple junction; 03, 14) hydride: hydrogen source; 04) heater; 05) ampoule (brass); 06) fixatives (pyrophyllite); 07, 16) electrical input; 12) ampoule (teflon); 13) glass wool; 15) ampoule cover (teflon). All empty space in ampoules 05, 12 is filled with silicone.

which this method is used are shown in Fig. 2. The principle for containing hydrogen is the same here as that described above using the first variant of the Polish chambers,<sup>22,23</sup> but an external source is no longer required to fill the ampoule with hydrogen: the hydrogen is liberated by thermally activated decomposition of a hydride (03, 14), placed beforehand into the lower part of the ampoule. Elimination of the corresponding injection system from this scheme permits, as in the variant<sup>23,24</sup> of hydrogen compressing systems, complete utilization of the possibilities of ordinary hydrostatic high-pressure chambers, while the appreciable simplification in the construction (compare Figs. 2 and 1) permits production of cells of quite small dimensions (Fig. 2, cell 11–17) in order to place existing quasihydrostatic chambers into the working zone. It is the use of the quasihydrostatic chambers that made it possible to exceed the limit  $\sim 30$  kbar and to compress hydrogen up to 70 kbar. It should be noted that even the 70 kbar limit is achieved only by the possibilities of chambers that are available to us and not by the possibilities of the method used in Ref. 28. Readers interested in details of the application of this method should consult Ref. 29.

By the middle of the 1970s, there remained twelve transition elements in Mendeleev's table for which it was not possible to obtain hydrogen saturated phases: Mn, Fe, Co, Mo, Tc, Ru, Rh, W, Re, Os, Ir and Pt. The application of a new method for compressing hydrogen halved the number of such elements. Manganese, iron, cobalt, molybdenum, technetium, and rhodium hydrides were synthesized (simultaneously with specialists from the Polish People's Republic) (Table I). It was possible to increase the hydrogen content in nickel hydride up to  $n \approx 1.25$ , passing through the stoichiometric composition of NiH. It is evident from Table I that hydride forming transition metals up to the present time form a compact block, including completely the

TABLE I. Hydrides of transition metals.

VI	VII	VIII		
18, 39, 112, 12 CrH ε	31, 33, 25, 58, 27 MnH <sub>0.95</sub> ε	37 FeH <sub>0.81</sub> ε	53 CoH <sub>0.51</sub> ε	19, 22, 45, 16, 32, 31 NiH <sub>1.25</sub> γ
10, 41 MoH ε	38, 33 TcH <sub>0.83</sub> ε	Ru	38, 113 RhH <sub>0.85</sub> γ	43; See Ref. 30 PdH γ
W	Re	Os	Ir	31 Pt

The maximum attained hydrogen content is indicated; ε are hydrides with hcp metal sublattice; γ are hydrides with fcc sublattice; the number of references in which the hydrides were synthesized and the phase diagrams of the corresponding Me-H systems were studied are presented in the upper left of the squares.

elements in the 3d series and with the exception of ruthenium, those of the 4d series as well. This creates favorable conditions for systematic study of the effect of hydrogen on the properties of such metals, especially considering the fact that metals situated close to one another in Mendeleev's table form wide regions of continuous solid solutions. For this reason, an appreciable number of alloys based on elements in groups VI–VIII, whose saturation by hydrogen was also made possible by high-pressure technology, was investigated together with the elements themselves.

All the hydrides studied have the typical metallic conductivity of the order of the conductivity of the starting metal (alloy). The kinetics of hydrogen absorption (formation of hydride) varies from metal to metal over an extremely wide range: at  $T = 250^\circ\text{C}$ , from several minutes for palladium<sup>30,31</sup> and nickel<sup>31,32</sup> to tens of hours for technetium<sup>33</sup> (the specimens are a foil with a thickness of 0.1–0.2 mm). The same diversity is also observed for the kinetics of thermal decomposition of hydrides into the metal and molecular hydrogen under atmospheric conditions: manganese<sup>34,35</sup> and technetium<sup>36</sup> hydrides are metastable at  $20^\circ\text{C}$ , while iron<sup>37</sup> and rhodium<sup>38</sup> hydrides decompose rapidly beginning at  $T \sim -100^\circ\text{C}$ . In liquid nitrogen, all hydrides without exception last indefinitely. Systems for "quenching" specimens were developed taking into account the kinetics of formation and decomposition of hydrides: first, the specimen is saturated with hydrogen at high pressure and temperature and, then, without changing the pressure, the specimen is rapidly cooled (if necessary, down to  $180^\circ\text{C}$ ), the pressure is decreased to atmospheric pressure, and the specimen is removed from the chamber for further study of physical properties. The investigation of these metastable (relative to the decomposition into the metal and molecular hydrogen) hydrides at atmospheric pressure added a great deal to the results of measurements at high hydrogen pressure. However, before going on to examining the physical properties of Me-H systems, it is necessary to describe at least briefly the basic variants of phase equilibria observed in these systems.

The point is that in many Me-H systems, phase transformations, accompanied by abrupt changes in the hydrogen concentration and all physical properties, occur. In addition, under the experimental conditions,

hydrogen-saturated phases (hydrides) often form side series of nonstoichiometric solid solutions. When a solid solution of hydrogen in a metal is in thermodynamic equilibrium with excess molecular hydrogen (which occurs for measurements performed under high hydrogen pressure), this does not lead to significant difficulties in interpreting the results of the measurements, since according to the phase rule, only single phase regions can exist on the  $T$ - $P_{\text{H}_2}$  diagrams of Me-H systems and it is only necessary to take into account the fact that even within such regions, the hydrogen concentration in the solution depends on the temperature and pressure. If, on the other hand, the Me-H solution is cooled to a temperature when the exchange of hydrogen with the surrounding medium is stopped (such a situation is realized in studying hydrogen presaturated specimens at atmospheric pressure), then in accordance with the metastable  $T$ - $c$  diagram (at a given pressure), it can also transform into a two-phase state. Thus, in order to interpret correctly the physical properties of Me-H systems, it is necessary to have reliable data on their phase composition for different values of the external parameters.

### 3. PHASE EQUILIBRIA IN METAL-HYDROGEN SYSTEMS

Hydrides of group VI–VIII transition metals and their alloys, independently of the starting structure of the metal, are formed on a base of one of the two closest packings of metal atoms, namely, hcp (ε) or fcc (γ) (see Table I), in which hydrogen occupies interstitial positions.<sup>1)</sup> Correspondingly, the formation of hydrides under high hydrogen pressure can be accompanied by a polymorphic (Cr-H,<sup>39</sup> Mn-H<sup>34,35</sup> Fe-H,<sup>37</sup> and Mo-H<sup>40</sup> systems) or isomorphic (Ni-H,<sup>22</sup> Tc-H,<sup>36,33</sup> Rh-H,<sup>38</sup> and Pd-H<sup>30</sup> systems) transformation of the metallic sublattice.

We shall illustrate the first possibility using as an example the system Mo-H. Under normal conditions, molybdenum has a bcc structure. Molybdenum hydride forms on a basis of an hcp metal sublattice. The  $T$ - $P_{\text{H}_2}$  phase diagram of the system Mo-H<sup>41</sup> is presented in Fig. 3.

The letter α indicates the region of existence of solid solutions of hydrogen on the bcc base of the molybdenum sublattice. In the range of pressures and temperatures studied, the hydrogen concentration in the α solution remains very low, while the composition of the ε phase (hydride) is close to the stoichiometric compo-

<sup>1)</sup>Here and subsequently we are dealing with massive specimens. In the case of specimens in the form of thin films, it is apparently possible for hydrides with other structures to form as well. For example, in Ref. 21, it is reported that heating a palladium film with thickness 500–1000 Å up to  $T \geq 600^\circ\text{C}$  in a hydrogen atmosphere at  $P_{\text{H}_2} = 1$  bar leads to the appearance of the hydride PdH<sub>1.33</sub> with a tetragonal metal lattice whose parameters at room temperature are  $a = 2.896 \text{ \AA}$ ,  $c = 3.330 \text{ \AA}$  (Semiletov *et al.*<sup>21</sup> initially obtained such a hydride by implanting hydrogen into palladium). With similar working of massive specimens, the usual Pd-H solutions with fcc metal sublattice were obtained.

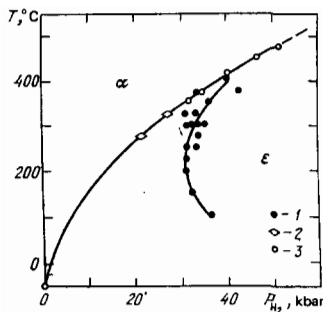


FIG. 3.  $T$ - $P_{H_2}$  phase diagram for the Mo-H system.<sup>41</sup> 1)  $\alpha \rightarrow \epsilon$  transition points;  $T = \text{const}$ ; 2)  $\epsilon \rightarrow \alpha$  transition,  $T = \text{const}$ ; 3)  $\epsilon \rightarrow \alpha$  transition,  $P_{H_2} = \text{const}$ .

sition of MoH.<sup>40</sup> It is evident from Fig. 3 that with increasing temperature, the boundary of the region of stability of the hydride (the transition  $\epsilon \rightarrow \alpha$ ) shifts to higher pressures, while the hysteresis of the transformation  $\alpha \rightleftharpoons \epsilon$  decreases. The pattern of the phase equilibria in other Me-H systems, where the formation of the hydride is likewise accompanied by a polymorphic transition of the metallic sublattice, is similar. For example, as in the  $\alpha$  phase of the Mo-H system, the solubility of hydrogen is low in the  $\alpha$  phases of the systems Cr-H<sup>39</sup> and Fe-H<sup>37</sup> and in the phase based on the  $\alpha$ -Mn structure in the Mn-H system.<sup>34,35</sup> The  $T$ - $P_{H_2}$  phase diagram of the Cr-H system<sup>42</sup> is completely analogous to the diagram of the Mo-H system<sup>41</sup> and is only shifted toward lower pressures. The formation and decomposition of hydrides in all these systems are accompanied by sharp changes in the electrical resistance. Typical isotherms  $R(P_{H_2})$  for the Mo-H system are shown in Fig. 4.

In this review, we concentrate primarily on the properties of Me-H systems of another type, where the formation of hydrides is accompanied by an isomorphic transformation of the metallic sublattice. It is interesting that the first metal-hydrogen system, which attracted the attention of researchers, namely, the Pd-H system belongs to precisely this type.<sup>43,30</sup> At room temperature, an increase in the hydrogen pressure leads first to a monotonic increase of the solubility of hydrogen in palladium up to  $n \approx 0.008$  (a  $\gamma_1$  solution of

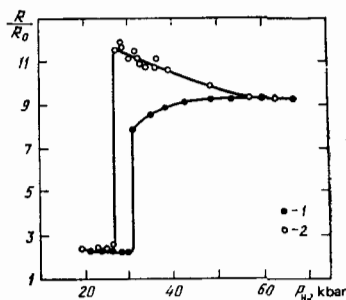


FIG. 4. Isotherms of electrical resistance of molybdenum in a hydrogen atmosphere at  $T = 325^\circ \text{C}$ .<sup>41</sup> 1) with increase in pressure; 2) with decrease in pressure.  $R_0$  is the resistance of a specimen at atmospheric pressure and room temperature.

Pd-H is formed). At  $P_{H_2} \sim 50$  torr, there is a phase transition and the concentration of the Pd-H solution increases abruptly to  $n \approx 0.6$  (a  $\gamma_2$ -hydride solution is formed). With further increase in pressure, the solubility of hydrogen in palladium increases monotonically up to  $n = 1$ . The  $\gamma_1$  and  $\gamma_2$  phases have, as in the starting palladium, a fcc metal lattice, but with a larger spacing. As the temperature increases, the pressure of the transformation  $\gamma_1 \rightleftharpoons \gamma_2$  increases, while the abrupt change in the solubility decreases, and at  $T_{cr} = 292^\circ \text{C}$ ,  $(P_{H_2})_{cr} = 19.7$  bar the curve of this transformation on the  $T$ - $P_{H_2}$  diagram terminates at the critical point. On the  $T$ - $c$  projection of the  $T$ - $P_{H_2}$ - $c$  phase diagram, this corresponds to the presence of a hump for  $T < T_{cr}$  corresponding to stratification into isomorphic phases  $\gamma_1$  and  $\gamma_2$ , depleted and enriched with hydrogen, and for  $T > T_{cr}$ , to regions of continuous solid Pd-H solutions.

Phase transformations in the Pd-H system occur in a range of pressures and temperatures that is convenient for measurements and has been assimilated a long time ago. At the present time, it is one of the most studied systems and it is a classical example of a Me-H system, separating into isomorphic phases. Investigations at high hydrogen pressures revealed a number of systems of this type, among which the closest analog to the Pd-H system is the Ni-H system. Its  $T$ - $P_{H_2}$  phase diagram is presented in Fig. 5. In contrast to palladium, nickel is a ferromagnet with a Curie point at  $T_c \approx 354^\circ \text{C}$  and in the region of existence of the  $\gamma_1$  phase, the  $T$ - $P_{H_2}$  diagram of the Ni-H system has an additional curve of Curie points above which solutions are paramagnetic and below which they are ferromagnetic ( $\gamma_2$  solutions are paramagnetic down to liquid helium temperature<sup>44</sup>). As far as the transformation  $\gamma_1 \rightleftharpoons \gamma_2$  is concerned, as in the Pd-H system, the pressure of the transitions  $\gamma_1 \rightarrow \gamma_2$  and  $\gamma_2 \rightarrow \gamma_1$  increases with increasing temperature. The hysteresis of the transformation decreases slowly down to the intersection of the curve of the transition  $\gamma_1 \rightarrow \gamma_2$  with the curve formed by the Curie points of the  $\gamma_1$  phase at  $T \sim 270^\circ \text{C}$ , and then disappears. In the range  $350 < T_{cr} < 430^\circ \text{C}$  and  $16 < (P_{H_2})_{cr} < 19$  kbar, the curve of the transformation  $\gamma_1 \rightarrow \gamma_2$  terminates at the critical

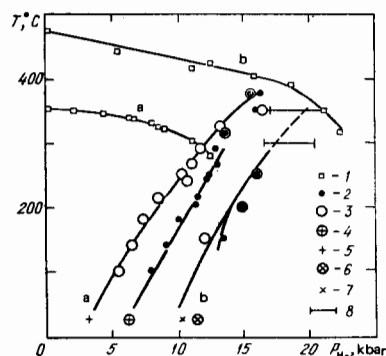


FIG. 5.  $T$ - $P_{H_2}$  phase diagrams of the systems Ni-H (a)<sup>32</sup> and  $\text{Ni}_{90}\text{Fe}_{10}$ -H (b).<sup>48</sup> 1) Curie points; 2) pressure of the transitions  $\gamma_1 \rightarrow \gamma_2$ ; 3)  $\gamma_2 \rightarrow \gamma_1$ ; 4, 5) pressure of these transitions according to Refs. 46 and 45; 6, 7) obtained by interpolating the data in Ref. 46; 8) regions of supercritical anomalies in the electrical resistance.

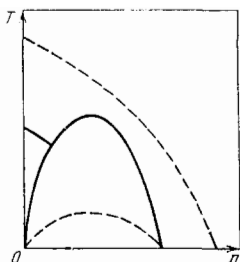


FIG. 6. Schematic diagram of the  $T$ - $c$  projection of  $T$ - $P_{H_2}$ - $c$  phase diagrams of Ni-H (continuous lines) and  $Ni_{90}Fe_{10}$ -H (dashed lines) systems.

point. The  $T$ - $c$  projection of  $T$ - $P_{H_2}$ - $c$  phase diagram of the Ni-H system is illustrated schematically in Fig. 6. We emphasize that this is precisely the projection of the volume  $T$ - $P_{H_2}$ - $c$  diagram (on the surface  $P_{H_2} = \text{const}$ ), since equilibrium between the phases  $\gamma_1$  and  $\gamma_2$  with compositions  $n_{\gamma_1}^{\text{max}}$  and  $n_{\gamma_2}^{\text{max}}$  at each chosen temperature corresponds to its own hydrogen pressure. For example, at room temperature,  $3.4 < P_{H_2} < 6.3$  kbar<sup>45,46</sup> while at the critical point  $16 < (P_{H_2})_{\text{cr}} < 19$  kbar,<sup>32</sup> see Fig. 5. In reality, the hump corresponding to stratification into  $\gamma_1$  and  $\gamma_2$  phases is very asymmetrical: the minimum solubility of hydrogen in the  $\gamma_2$  phase varies from  $n_{\gamma_2}^{\text{min}} \approx 1$  at room temperature<sup>26,32</sup> to  $n_{\gamma_2}^{\text{min}} \leq 0.7$  at  $T = 350^\circ\text{C}$ ,<sup>32</sup> while the maximum solubility of hydrogen in the  $\gamma_1$  phase at  $T = 350^\circ\text{C}$  constitutes  $n_{\gamma_1} \leq 0.02$ .<sup>32</sup>

The significant decrease in the Curie point of the  $\gamma_1$  phase (by  $\approx 76^\circ\text{C}$ ) of the Ni-H system relative to the Curie point of nickel when the hydrogen pressure is increased to 12.5 kbar is interesting in connection with the small solubility of hydrogen in the  $\gamma_1$  phase of the Ni-H system (see Fig. 5). In an inert medium at  $P = 12.5$  kbar, the Curie point of nickel increases by  $\approx 4^\circ\text{C}$  (see Ref. 47). Therefore, the observed decrease in  $T_c$  of the  $\gamma_1$  phase is due to the increase in the hydrogen concentration in nickel in proportion to the increase in the hydrogen pressure with the effect, reaching  $\approx (76 + 4)^\circ\text{C} \approx 0.13 T_c^{\text{Ni}}$  at  $P_{H_2} = 12.5$  kbar, being caused by the penetration of only  $n \leq 0.02$  hydrogen into nickel.

The high sensitivity of Curie points to the hydrogen content in solid solutions based on nickel and its alloys permitted using in many cases the experimental dependences  $T_c(P_{H_2})$  and  $T_c(n)$  to clarify the topology of the phase diagrams. The most vivid example is the proof of the termination of curves of the isomorphic transformation  $\gamma_1 \rightleftharpoons \gamma_2$  on  $T$ - $P_{H_2}$  phase diagrams of Ni-Fe-H solutions at the critical points<sup>48</sup> [the position of the critical point in the Ni-H system indicated above was obtained by extrapolating the dependences  $T_{\text{cr}}$  and  $(P_{H_2})_{\text{cr}}$  in the Ni-Fe-H system on the content of iron in the starting Ni-Fe alloys]. It should be noted that the experimental proof of the existence of a critical point on the curve of a first order phase transition in principle is a complicated problem, so that we shall consider it in somewhat greater detail.

The Ni-Fe alloys containing up to  $\sim 70$  at.% Fe, can have a fcc structure; hydrogen solutions based on them

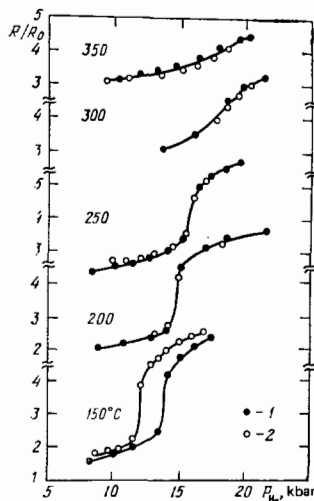


FIG. 7. Isotherms of electrical resistance for the  $Ni_{90}Fe_{10}$  alloy in a hydrogen atmosphere.<sup>48</sup> 1) Points, measured with an increase in pressure; 2) with a decrease in pressure.  $R_0$  is the resistance of a specimen at  $25^\circ\text{C}$  and  $P = 1$  bar.

also have the same metallic structure. The position of the critical points was studied for hydrogen solutions in alloys with 5, 10 and 15 at.% Fe. Figure 7 shows the isotherms of equilibrium values of the electrical resistance of the Ni-Fe alloy with 10 at.% Fe in a hydrogen atmosphere. At  $T = 150^\circ\text{C}$ , the transformation  $\gamma_1 \rightarrow \gamma_2$  has appreciable hysteresis, i.e., it is well known to be a first-order phase transition accompanied by an abrupt change in the volume and solubility of hydrogen. Beginning at  $\sim 200^\circ\text{C}$ , the transformation becomes hysteresis-free. At  $250^\circ\text{C}$ , the transition becomes appreciably diffuse, while at 300 and  $350^\circ\text{C}$ , the abrupt change in the resistance disappears and the  $R(P_{H_2})$  curves assume a form that is typical for resistance isotherms in the supercritical region. Thus, the behavior of the electrical resistance permits one to assume that the curve of the transformation  $\gamma_1 \rightleftharpoons \gamma_2$  on the  $T$ - $P_{H_2}$  diagram of the  $Ni_{90}Fe_{10}$ -H system terminates at the critical point and, in addition,  $250 < T_{\text{cr}} < 300^\circ\text{C}$ .

As the iron concentration in Ni-Fe alloys increases, the curves of the transformation  $\gamma_1 \rightleftharpoons \gamma_2$  shift toward higher pressures, while the critical temperatures of the stratification into  $\gamma_1$  and  $\gamma_2$  decrease. The curves of the transformation  $\gamma_1 \rightarrow \gamma_2$  and  $\gamma_2 \rightarrow \gamma_1$  for the alloy with 10 at.% Fe, constructed from measurements of the electrical resistance, are presented in Fig. 5. This figure also presents the dependence of the Curie point of this alloy on the hydrogen pressure. The advantageous mutual positioning of the  $T_c(P_{H_2})$  curve and the curve of the transformation  $\gamma_1 \rightleftharpoons \gamma_2$  is what allows one to show rigorously that this transformation terminates at the critical point. Indeed, the Curie point curves must be discontinuous when the curves of the first-order phase transitions  $\gamma_1 \rightarrow \gamma_2$  and  $\gamma_2 \rightarrow \gamma_1$  intersect because the Curie temperature of the solution is a continuous function of its concentration, while the concentration at these transitions changes in a discontinuous manner. For example, the curve of the Curie points for nickel terminates on the line of the transition  $\gamma_1 \rightarrow \gamma_2$  at  $\sim 270^\circ\text{C}$

(see Fig. 5); therefore, in this case,  $T_{cr} > 270^\circ\text{C}$ . The curve  $T_c(P_{H_2})$  for the alloy with 10 at.% Fe goes over into the  $\gamma_2$  region, smoothly intersecting the continuation of the curve of the transformation  $\gamma_1 \rightarrow \gamma_2$  in the supercritical region with  $T \sim 360^\circ\text{C}$ ; therefore, this curve lies significantly higher than the region of critical phenomena and  $T_{cr} \ll 360^\circ\text{C}$ . The evolution of the  $T$ - $c$  projection of the phase diagram of the Ni-Fe-H system with a transition from Ni to the alloy  $\text{Ni}_{90}\text{Fe}_{10}$  is shown schematically in Fig. 6.

With an atomic fraction of iron  $0.15 < x_{Fe} < 0.4$  in the Ni-Fe alloys, the critical temperature of stratification of the Ni-Fe-H solid solutions drops below  $25^\circ\text{C}$ .<sup>46,48</sup> In  $\gamma$  alloys with a higher iron concentration, the hydrogen solubility for  $T > 25^\circ\text{C}$  must thus be a continuous function of pressure, which was confirmed experimentally with alloys with 66.1 and 67.5 at.% Fe in Refs. 49 and 50, once again in the course of studying the dependences  $T_c(P_{H_2})$  (see subsection b, 1 in Sec. 4). The investigation of systems forming wide regions of continuous solid solutions is, naturally, most informative, since in this case it is possible to observe systematically the dependence of the properties of specimens on the hydrogen content. From this point of view, together with the Ni-Fe alloys, the nickel alloys with Cu, Mn, Cr, and alloys of the pseudobinary Invar system  $\text{Fe}_{65}(\text{Ni}_{1-x}\text{Mn}_x)_{35}$  (see Ref. 51 for a discussion and references) and a number of alloys based on palladium (with Cu, Ag, Au, Pt, Ir, and others; see references in Refs. 30 and 52), for which both the concentration intervals of existence of continuous solid solutions of hydrogen and the mutual solubility of metallic components are high, are also convenient objects for studying the  $\gamma$  solutions of hydrogen.

The capability to form wide regions of continuous solid solutions with hydrogen is not, however, the exclusive privilege of alloys. Thus, at  $T = 225^\circ\text{C}$ , the concentration of  $\epsilon$  solutions Co-H increases monotonically with hydrogen pressure, reaching  $n = 0.51$  at  $P_{H_2} = 65$  kbar.<sup>53</sup> The isotherm  $T = 300^\circ\text{C}$  of the solubility of hydrogen in technetium (Fig. 8) is interesting. Two regions of supercritical anomalies (near  $P_{H_2} = 3$  and 13 kbar) of two isomorphous phase transformations terminating at critical points for  $T < 300^\circ\text{C}$  can be clearly seen on it.

Since the investigation of precisely such nonstoichi-

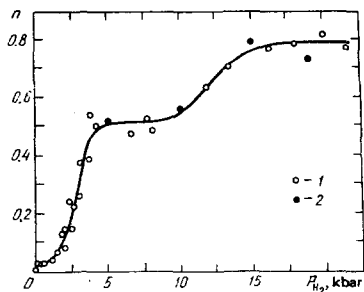


FIG. 8. Solubility of hydrogen in technetium at  $T = 300^\circ\text{C}$ . 1) Data in Ref. 36; 2) data in Ref. 33.

ometric phases of Me-H at high pressure is, as already noted, of considerable interest, while many of their properties can, for the time being, be studied only at atmospheric pressure and, as a rule, at low temperatures (in order to avoid losses of hydrogen from the specimens), it is necessary to make some remarks concerning the interpretation of data obtained at atmospheric pressure and their relation to the measurements at high hydrogen pressure and high temperatures. The first thing that comes to mind, considering that the configurational entropy should be a minimum, is that the nonstoichiometric Me-H solutions cannot be thermodynamically stable down to  $T = 0$  K and as the temperature decreases, they must undergo either a decomposition into a phase with stoichiometric composition or they must become ordered. This situation is realized, for example, for hydrogen solutions in group V transition metals (see Refs. 5 and 54). In the case of hydrogen solutions based on transition metals in groups VI-VIII, an anomalous behavior of the physical properties with decreasing temperature is observed only for palladium hydride ( $n \sim 0.6-0.8$ ,  $T \lesssim 55\text{K}$ ; see Ref. 30) and is probably related to its atomic ordering (see, for example, Refs. 55-57), although, we must admit that the data obtained by different researchers concerning the nature of this ordering are poorly correlated. For other solutions, in the absence of a trivial stratification into isomorphous (and, as a rule, also nonstoichiometric) phases, such phenomena have not yet been observed. It is possible that this is related to the fact that the corresponding critical temperatures are very low and thermodynamically equilibrium states are not attained for kinetic reasons.

Further, when studying high pressure phases in Me-H systems, depending on the experimental conditions, it is necessary to distinguish clearly between two types of thermodynamic equilibrium: 1) stable equilibrium between a solid solution and excess hydrogen, which is established with measurements in a hydrogen atmosphere, when the temperature is sufficiently high for exchange of hydrogen between the solid solution and the molecular phase; 2) metastable equilibrium with fixed total hydrogen content in the specimen, which is established if the temperature is sufficiently low to retard the liberation of hydrogen from the specimen, but sufficiently high to ensure diffusion redistribution of hydrogen within the specimen (for example, with stratification of the solid solution into isomorphous phases). It turns out that the  $T$ - $c$  section of the phase diagram of metastable equilibria can differ greatly from the  $T$ - $c$  projection of the  $T$ - $P_{H_2}$ - $c$  diagram of stable equilibria. For example, in the Ni-H system at room temperature and high hydrogen pressure (when conditions for stable thermodynamic equilibrium are realized), the boundary of the hump corresponding to stratification into  $\gamma_1$  and  $\gamma_2$  phases  $n_{\gamma_2}^{min} \geq 1$ ,<sup>26,32</sup> while for  $T < -20^\circ\text{C}$  and  $P = 1$  bar<sup>44</sup> (when liberation of hydrogen from specimens is kinetically prevented and metastable equilibrium conditions are realized), the minimum hydrogen content in the  $\gamma_2$  phase already constitutes  $n_{\gamma_2}^{min} = 0.7 \pm 0.05$ . Another example is the lowering of the critical temperature for the stratification  $\gamma \rightarrow \gamma_1 + \gamma_2$  with a transition from

stable to metastable equilibria in the  $\text{Ni}_{60}\text{Cu}_{40}\text{-H}$  system from  $T_{\text{cr}} > 100^\circ\text{C}$  to  $T_{\text{cr}} < -50^\circ\text{C}$  (for more detail see Ref. 51). Thus, establishing a relation between the two sets of data usually obtained for high-pressure phases (at high hydrogen pressure and at atmospheric pressure) requires special analysis in each specific case.

The last problem that should be examined in this section concerns the volume effects accompanying dissolution of hydrogen in transition metals. The formation of hydrides at high hydrogen pressure can be accompanied by an appreciable increase in the volume of the specimens  $V$ . For example, with the formation of  $\epsilon$  hydrides  $\text{CrH}$ ,<sup>39</sup>  $\text{MoH}$ <sup>40</sup> and  $\text{FeH}_{0.8}$ ,<sup>37</sup> the volumes increase by  $\approx 19$ , 20 and 16%, respectively. In the case of manganese<sup>53</sup> and cobalt<sup>53</sup> which form wide regions of continuous  $\epsilon$  solutions with hydrogen, the volumes of these solutions likewise increase in proportion to the increase in the hydrogen concentration and, in addition, approximately linearly. An interesting dependence  $V(n)$  at atmospheric pressure and room temperature is observed for  $\epsilon$  solutions Tc-H. According to x-ray analysis data,<sup>33</sup> the hydride volume exceeds the volume of the starting technetium by  $\approx 6.4\%$  and does not change over a wide range of hydrogen concentrations  $0.385 \leq n \leq 0.78$ .

The dependence  $V(n)$  for  $\gamma$  hydrogen solutions in palladium, nickel, and a large number of alloys based on them are very similar; see Fig. 9, wherein the dependences  $\Delta V_0(n) = V(n) - V(0)$ , where  $V(n)$  and  $V(0)$ , namely, the volumes of the unit cells of the metal with a hydrogen content of  $n$  and without hydrogen, are presented. It can be seen that the volumes of the solutions increase with increasing  $n$  and, in addition, all dependences (where, of course, the effect exceeds the limits of error in the measurements) have a general property: for  $n \geq 0.7-0.8$ , their slope  $\beta = (\partial/\partial n)\Delta V_0(n)$  is observed to decrease. For example, for the alloys  $\text{Ni}_{80}\text{Fe}_{20}$  and  $\text{Ni}_{32.5}\text{Fe}_{67.5}$ , the slope changes from  $\beta \approx 9.5 \text{ \AA}^3$  for  $n < 0.8$  to  $\beta \approx 2.5 \text{ \AA}^3$  for  $n > 0.8$  (following Ref. 52, where the dependence  $\Delta V_0(n)$  was constructed for palladium alloys, we approximated the analogous dependence for nickel-iron alloys for  $n < 0.8$  and  $n > 0.8$  by straight line segments). The nature of this effect is not yet understood. Some possibilities for explaining it are opened up by the study of hydrogen solutions in alloys based on nickel, for which the compositions  $n > 1$  are obtained. Indeed,

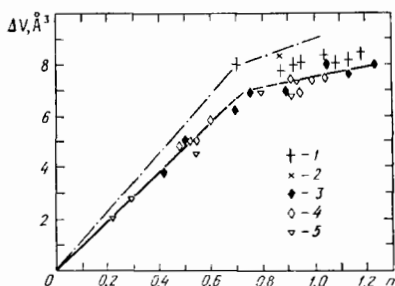


FIG. 9. The dependences  $\Delta V_0(n) = V(n) - V(0)$  (see Sec. 3). 1) Ni,  $T = 293 \text{ K}$ ,<sup>32</sup> 2) Ni,  $T = 293 \text{ K}$ ,<sup>114</sup> 3, 4) Ni-Fe alloys with 20 and 67.5 at.% Fe, respectively,  $T = 83 \text{ K}$ ,<sup>50</sup> 5)  $\text{Fe}_{65}\text{Ni}_{16}\text{Mn}_{29}$ ,  $T = 83 \text{ K}$ ,<sup>84</sup>; the dot-dash line indicates the analogous dependence for alloys based on palladium at room temperature.<sup>52</sup>

with  $n \approx 0.6$  and at room temperature, hydrogen in nickel occupies octahedral interstices,<sup>59</sup> whose number in a fcc lattice equals the number of sites. When all these interstices are filled, the  $\gamma$  hydride will have composition  $n = 1$ . Therefore,  $\gamma$  solutions with  $n > 1$  must be structurally different from solutions with  $n \approx 0.6$ . The only anomaly in the dependences  $\Delta V_0(n)$  for  $\gamma$  solutions Me-H at hydrogen concentrations up to  $n = 1.23$  (for the solution  $\text{Ni}_{80}\text{Fe}_{20}\text{-H}$ ) occurs at  $n \sim 0.8$  and it is reasonable to assume that it is related to the beginning of a structural rearrangement. As far as the rearrangement is concerned, it may involve, for example, filling for  $n > 0.8$  part of the tetrahedral interstices, which in a fcc lattice number two per site (although in this case, due to the smaller sizes of the tetrapores, the partial volume of hydrogen, characterized by the value of  $\beta$ , is more likely to increase rather than to decrease). It also cannot be excluded that for  $n > 1$  hydrogen continues to occupy only octahedral interstices, whose number relative to the number of sites increases due to an increase in the number of vacancies in a metal lattice for  $n > 0.8$ .<sup>2)</sup>

#### 4. MAGNETIC PROPERTIES OF METAL-HYDROGEN SOLUTIONS

A characteristic of group VI-VIII 3d metals and alloys based on them is the existence of magnetic order and the behavior of the magnetic properties with hydrogenation can serve as a convenient indicator of changes occurring in the electron subsystem. Experiments have shown that for transition metals the introduction of hydrogen does not lead to a unique change in their magnetic properties, for example, to a decrease in the temperature of transition into the magnetically ordered state, which is a dominant tendency in the case of hydrogenation of rare earth metals.<sup>62</sup> On the contrary, the effects have turned out to be very diverse. In particular, the following are observed on hydrogenation of pure metals.

Chromium, which has a bcc crystal structure, is an antiferromagnet with the Neel point at  $T_N = 312 \text{ K}$ ; the  $\epsilon$  hydride of chromium  $\text{CrH}_{0.97}$  is paramagnetic down to helium temperatures.<sup>63,64</sup> The low-temperature modification of manganese ( $\alpha\text{-Mn}$ ) is an antiferromagnet with  $T_N = 100 \text{ K}$ ; the  $\epsilon$  solutions Mn-H in the range of compositions  $0.65 \leq n \leq 0.94$  have a spontaneous magnetization, which increases monotonically as the hydrogen content in the solution increases, but even at  $n = 0.94$  it remains very small ( $\leq 0.02 - 0.05 \mu_B/\text{Mn atom}$  at  $T = 82 \text{ K}$ ;  $\mu_B$  is the Bohr magneton), while the Curie point reaches quite high values  $T_c > 280 \text{ K}$ .<sup>58</sup> Iron with a bcc

2) We note that the presence of wide regions of concentrations where the volume of the solution depends weakly on the content of the injected component (as happens, for example, in Pd-H and Ni-H solutions with  $n \geq 0.7$  or in Tc-H solutions with  $0.385 \leq n \leq 0.78$ ) is not a specific property of hydrogen solutions in particular. A small (for example, Zr-C) and even negative (Zr-N) change in volume with increasing concentration of the injected element were already observed previously in other solutions.<sup>61</sup> The reasons for this behavior of the volume in these systems also has not yet been established.

structure is a ferromagnet with  $T_c = 1043$  K, which has at  $T = 0$  K a spontaneous magnetization  $\sigma_0 = 2.22 \mu_B/\text{atom}$ ; the  $\epsilon$  hydride of iron  $\text{FeH}_{0.8}$  is also a ferromagnet and, in addition, with nearly the same value of the magnetization  $\sigma_0 = 2.2 \mu_B/\text{Fe atom}$  and with  $T_c \gg 80$  K.<sup>65</sup> Dissolution of hydrogen in the hcp modification of cobalt (ferromagnet,  $\sigma_0 = 1.72 \mu_B/\text{atom}$ ) leads to a small decrease in the spontaneous magnetization with initial slope  $\partial\sigma_0/\partial n|_{n=0} \approx -0.6 \mu_B/H \text{ atom}$ ; for  $n \geq 0.3$ , the dependence  $\sigma_0(n)$  flattens out.<sup>66</sup> Nickel, with a fcc structure, is a ferromagnet with  $T_c = 627$  K and  $\sigma_0 = 0.616 \mu_B/\text{atom}$ . Injection of hydrogen causes  $T_c$  to decrease (see Figs. 5 and 6) and  $\sigma_0$  to decrease as well; the  $\gamma_2$  solutions Ni-H, which are stable at atmospheric pressure and  $T < 250$  K in the range of concentrations  $0.7 \leq n \leq 1.18$ , are paramagnetic for  $T \geq 4.2$  K.<sup>44</sup>

It is already evident from this simple listing of properties that it is, in any case, not easy to construct a systematic picture of the effect of hydrogen on the magnetic properties of transition metals, limiting the study of Me-H solutions to the elements only. In this connection, it was very fruitful to investigate the solutions of hydrogen in fcc alloys of 3d metals and, primarily, in alloys based on nickel. For a long time, alloys based on nickel were a subject of intensive experimental investigations and extensive factual information, which gives a clear picture of the effect of alloying substitution elements on the magnetic properties, has been collected (see Refs. 67 and 68). Alloys form a wide range of continuous  $\gamma$  solutions with hydrogen, which permits following in a systematic manner the effect of alloying with hydrogen on these properties. Finally, the magnetic properties of fcc nickel alloys are correctly described by the band theory of magnetism, which provides a good foundation for interpreting the effects of hydrogenation.

#### a) Magnetic properties of Ni-Me alloys

In the band theory of magnetism, the electrons, which partially fill the conduction band, are the carriers of the magnetic moment. The exchange interaction causes the energy of the electrons to depend on the orientation of their spins relative to the total magnetic moment  $\sigma$ , which, in the first approximation, can be represented as a relative shift in the electron subbands for opposite directions of spin by the energy  $\Delta = I \cdot \sigma$ , where  $I$  is the effective exchange interaction parameter. Usually, it is assumed that in transition metals, the Fermi level intersects the overlapping narrow  $d$  band (with high density of electron states) and the wide  $s$  band (with low density of states), and in this case, the magnetic properties of the material are determined primarily by the structure of the  $d$  band and the degree to which it is filled. It should be noted that in spite of the evident roughness of these approximations, in the case of fcc alloys of 3d metals, such an approach permits describing quantitatively the temperature, field, pressure and concentration dependences of their macroscopic magnetic characteristics (see, for example, Refs. 76–70).

The concentration dependences of the spontaneous magnetization  $\sigma_0$  at  $T = 0$  K for fcc alloys of 3d metals

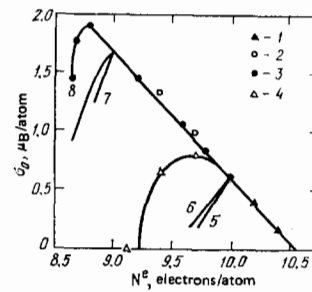


FIG. 10. Spontaneous magnetization  $\sigma_0$  at  $T = 0$  K as a function of the average number of electrons ( $3d+4s$ ) per atom  $N^e$  for binary fcc alloys.<sup>34</sup> 1) Ni-Cu; 2) Ni-Co; 3) Ni-Fe; 4) Ni-Mn; 5) Ni-Cr; 6) Ni-V; 7) Co-Cr; 8) Co-Mn.

is customarily represented in the form of the so-called Pauling-Slater curve (Fig. 10) as a function of the average number of  $3d+4s$  electrons  $N^e$  (present in the isolated atoms) per atom in the alloy. Figure 10 presents the experimental values of  $\sigma_0$  (agreeing well with data in the literature<sup>67,68</sup>) for Ni-Me alloys, serving as a basis for obtaining the solid hydrogen solutions examined in this review.

The following characteristic property of the Pauling-Slater curve is interesting: the values of  $\sigma_0$  for nickel alloys with copper, cobalt and iron (with  $x_{Fe} \leq 0.6$ ) fall on a single straight line with a slope  $\partial\sigma_0/\partial N^e \approx -1.05 \mu_B/\text{electron}$ . Nickel is well described by the band ferromagnetism model and, in addition, near  $T = 0$  K, it can be viewed as a strong band ferromagnet, for which one half of the  $d$  band ( $d\uparrow$  with spins pointing up) is filled completely, while the second half ( $d\downarrow$  with spins pointing down) is only partially filled.<sup>7</sup> This is shown schematically in Fig. 11a. The quantity  $\sigma_0$  is related to the number of electrons with uncompensated spin, i.e., in this case, simply to the number of holes  $p\uparrow$  in the  $d\downarrow$  subband, by the relation  $\sigma_0 = (1/2)g\mu_B p\uparrow \approx \mu_B p\uparrow$ , since for nickel (and alloys based on it) the spectroscopic factor  $g \approx 2.2 \sim 2$  (see Ref. 68) (which indicates the smallness of the orbital contribution, i.e., the practically pure spin origin of magnetization in these materials). The linear dependence  $\sigma_0(N^e)$  with

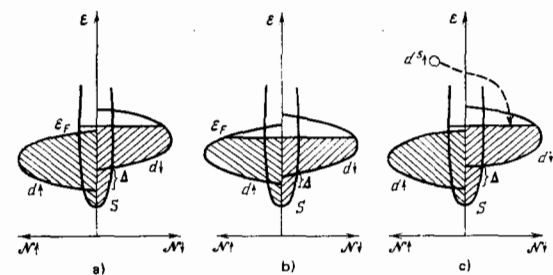


FIG. 11. Diagram of band structures of collectivized ferromagnets at  $T = 0$  K. a) strong ferromagnets; b) weak; c) diagram illustrating flow of electrons from virtual impurity bound state  $d^{\downarrow}$  into the  $d^{\downarrow}$  subband of a strong ferromagnet.  $\epsilon$  is the energy of the states;  $N^{\uparrow}$  and  $N^{\downarrow}$  are the density of states with spin pointing up and down;  $\epsilon_F$  is the Fermi energy;  $\Delta = I\sigma_0$ .

slope  $\partial\sigma_0/\partial N^e \approx -1 \mu_B/\text{electron}$  for nickel alloys with Cu, Co, and Fe are well explained if it is assumed<sup>67</sup> that alloying nickel with these elements 1) does not lead to deformation of the curves for the density of electron states  $\mathcal{N}^\uparrow(\varepsilon)$  and  $\mathcal{N}^\downarrow(\varepsilon)$ , only shifting them in energy, relative to one another as a single entity (this approximation is called the rigid band approximation for ferromagnets; the physical significance of this approximation and the limits of its applicability are discussed in detail in Ref. 71); 2) lets the ferromagnets remain strong (with completely filled  $d\uparrow$  subband). Indeed, in this case, the changes in  $\sigma_0$  accompanying alloying will stem primarily from the change in the number of holes in the  $d\uparrow$  subband and, therefore,

$$\sigma_0(x_{Me}) \approx \sigma_0^{Ni} - \Delta Z \mu_B x_{Me}, \quad (4.1)$$

where  $\Delta Z = Z_{Ni} - Z_{Me}$  is the difference between the nuclear charges of the nickel and impurity atoms, which is observed experimentally.

As can be seen from Fig. 10, the curve of  $\sigma_0(N^e)$  for many alloys deviates from the curve predicted by the rigid band model for strong collectivized ferromagnets. For Ni-Fe alloys with  $x_{Fe} \geq 0.63$ , this deviation is apparently related to the appearance of a significant number of holes both in the  $d\uparrow$  and in the  $d\downarrow$  subbands.<sup>72</sup> The corresponding band scheme is shown in Fig. 11b. The fact that for collectivized ferromagnets with holes in both  $d$  subbands at  $T=0$  K (such ferromagnets are called weak), the spontaneous magnetization may not increase, but rather decrease with increasing number of holes in the  $d$  band, can be illustrated as follows. Let, as in Fig. 11b,  $|\partial\mathcal{N}^\uparrow(\varepsilon_F)/\partial\varepsilon| > |\partial\mathcal{N}^\downarrow(\varepsilon_F)/\partial\varepsilon|$ , where  $\varepsilon_F$  is the Fermi energy. Then, when the degree of filling of the  $d$  band by electrons decreases, the number of holes in the  $d\uparrow$  subband will increase more rapidly than in the  $d\downarrow$  subband and  $\sigma_0 = (1/2)g\mu_B(p\uparrow - p\downarrow) \approx \mu_B(p\uparrow - p\downarrow)$  will decrease.

The "anomalous" dependences  $\sigma_0(N^e)$  of the type observed for Ni-Cr and Ni-V alloys, when the sharp deviation from a straight line with slope  $\partial\sigma_0/\partial N^e \approx -1 \mu_B/\text{electron}$  appears already at low concentrations of the alloying element, were explained by Friedel<sup>71</sup> using the concept of "virtual bound states." According to Friedel, when an atom of a transition impurity appears in a metal, the  $d$  level of this atom, which is higher than the energy of the bottom of the conduction band, becomes delocalized, but in the coordinate-energy space remains a "virtual  $d$  level," namely, the region where 1) the amplitude of the spherical component of the wave function with  $l=2$  is anomalously large and 2) this amplitude corresponds to the excess charge density, which, being summed over the entire region, approximately equals the charge of the starting bound  $d$  state (multiply degenerate,  $2l+1=5$ ). This virtual level can split into sublevels with oppositely oriented spin due to the intra-atom exchange interaction, if the metal-solvent has a sufficiently narrow conduction band (and, especially, is a ferromagnet itself).

In the case of nickel, as long as the virtual  $d^{5\uparrow}$  sublevel lies below the Fermi energy, alloying will lead to changes in the rigid band model for strong collectivized

ferromagnets (4.1). This is due to the fact that screening of the excess impurity charge must be responsible, primarily, for part of the  $d$  band with high density of states at the Fermi level, i.e., the  $d\uparrow$  subband; in addition, the characteristic screening radius is less than or of the order of the interatomic distance.<sup>71</sup> Therefore, the magnetic moments of the nickel matrix and of the impurity should not depend on the impurity concentration:

$$\begin{cases} \mu_{\text{matrix}} = \text{const}, \\ \mu_{\text{imp}} \approx \mu_{\text{matrix}} - \Delta Z \mu_B, \end{cases}$$

which for the average magnetic moment of the alloy  $\bar{\mu} = \sigma_0$  leads to Eq. (4.1).

As  $\Delta Z$  increases (i.e., the farther the impurity element is to the left of nickel in Mendeleev's table), the perturbing potential introduced by the impurity, which is a repulsive, increases. It may be expected that for some value of  $\Delta Z$  this potential will be large enough to remove locally the virtual  $d^{5\uparrow}$  state from the filled half of the  $d$  band and move it in energy above the Fermi level. This situation is schematically illustrated in Fig. 11c. Electrons from such a state flow into the conduction band and primarily enter the  $d\uparrow$  subband with opposite spin orientation due to its high density of states at the Fermi level (dashed line in Fig. 11c). The state with  $d=2$  is five-fold degenerate. Therefore, when the Fermi level is crossed by the virtual  $d^{5\uparrow}$  level, five electrons from states with spin pointing up go over into a state with spin pointing down, which changes the spontaneous magnetization by  $\approx 10\mu_B$ . This leads to the following equation for the average magnetic moment of the alloy:

$$\sigma_0(x_{Me}) \approx \sigma_0^{Ni} + (\Delta Z - 10) \mu_B x_{Me}, \quad (4.2)$$

which agrees well with the slopes of the dependences  $\sigma_0(N^e)$  for alloys of nickel with chromium, vanadium and titanium.

Thus, if the impurities are listed in order of decreasing atomic numbers, the following pattern is observed when nickel is alloyed with other 3d metals. Copper, cobalt, iron and (partially) manganese do not change the band structure of nickel very much and over a wide range of compositions of the alloys, the dependences  $\sigma_0(x_{Me})$  are determined primarily by changes in the electron concentration  $N^e$ . With alloying by elements with  $Z \leq Z_{Cr}$ , both changes in  $N^e$  and in the band structure play an important role.

## b) Ni-Me-H solutions

As already noted, in order to interpret the properties of transition metal hydrides, for many years, and with variable success, two alternative models, namely the anion and proton models, were used. In the first model, the hydrogen in the metal was assumed to be a negatively charged ion  $H^-$ , while in the second it was assumed to be a proton  $H^+$ . From the point of view of the rigid band model, this meant the following. In the anion model, narrow bands, formed by electron levels of hydrogen, lie below the Fermi energy of the metal-sol-

vent. Since the hydrogen atom has a single electron, while each energy state in the band can be occupied by two electrons with oppositely oriented spin, these bands (one band for each hydrogen atom in a unit cell) are half filled. The missing electrons are taken from the conduction band of the starting metal (one electron per H atom). In the proton model, the hydrogen bands lie above the Fermi level of the metal-solvent and the electrons from these bands (one electron per H atom) flow into the conduction band of the metal.

The fact that in spite of intensive study of transition metal hydrides over many decades, it was not possible to make a final choice even between these two diametrically opposed models is due primarily to the hydrogenated metals (Pd and elements in the subgroups Ti and B having no physical properties that are uniquely related to the degree to which their conduction bands are filled (this problem is discussed in detail in Ref. 73). As can be seen from the preceding section, in the case of hydrogenation of fcc nickel alloys, magnetic properties, which permit studying experimentally the status of hydrogen in these objects, could serve as such an indicator. Indeed, for example, when strong collectivized ferromagnets (the alloys Ni-Cu, Ni-Co, Ni-Fe with  $x_{Fe} \leq 0.6$ ) are saturated with hydrogen, in view of the high density of states of the  $d\uparrow$  subband at the Fermi level, it is its degree of filling that will primarily change. If the anion model is valid, then the spontaneous magnetization must increase with slope  $\partial\sigma_0/\partial n \approx 1\mu_B/H$  atom, and if the proton model is valid,  $\sigma_0$  will decrease with slope  $\partial\sigma_0/\partial n \approx -1\mu_B/H$  atom.

At the present time, however, both these models, namely, the anion and proton models, are too rough and naive. Friedel's analysis<sup>74</sup> of the conditions for screening of the proton in transition metals showed that the state of hydrogen in metals at the beginning of the d series must be close to  $H^-$ , while in metals at the end of the series, to  $H^+$ . In recent years, a series of quantum mechanical calculations of the band structure of 3d and 4d metal hydrides, among which the seminal work performed by Switendik<sup>10</sup> should be specially noted, have been performed. The results of all the calculations, which, in addition, were performed using different methods (associated plane waves<sup>11-13</sup> and model Hamiltonian<sup>14</sup>) with a different choice of crystalline potentials and self-consistent calculations,<sup>11,12</sup> agree with one another satisfactorily and give for  $\gamma$  and  $\epsilon$  solutions with  $n \leq 1$  the following picture of the effect of hydrogen on the band structure of the metal. In order to describe hydrides of elements at the end of the 3d and 4d series, the anion model is completely inapplicable: a new hydrogen band below the Fermi level is not formed in such hydrides. The idea of "protonization" of hydrogen is more useful, but it also does not correctly describe the phenomena occurring, since the dissolved hydrogen strongly deforms the band structure of the metal and, in addition, both H-Me and H-H interactions play an important role. This deformation, however, has a selective character. States with d symmetry change little, while the energy of the s states decreases significantly. The latter leads to an increase in the number of states below the Fermi energy of the metal-solvent

with an increase in the number of protons in its interstices. Thus, part of the electrons ( $\eta \sim 0.4-0.1$  electrons/proton for Pd and Ni<sup>10</sup>), contributed by hydrogen atoms to the conduction band, fills the space above the Fermi level, while part goes into the additional levels below it. This effect can be qualitatively illustrated with the help of the diagrams in Fig. 11, assuming that as the hydrogen concentration in the metal increases the density of s states is shifted down in energy relative to the densities of  $d\uparrow$  and  $d\downarrow$  states.

Calculations of the band structures of hydrides of transition metals have explained, and in many cases quantitatively, the results of the experimental study of the electron heat capacity, magnetic permeability, photoemission spectra, and other physical properties, including superconductivity, of a number of Me-H systems; see Refs. 10-12, 14, and 30. In the case of Ni-Me-H solutions, these calculations have served as a theoretical basis for justifying the assumptions for describing their magnetic properties in the "rigid d band" model,<sup>75</sup> assuming that the change in these properties accompanying hydrogenation stems primarily from the increase in the degree of filling of the d band in the metal-solvent by electrons and, in addition, the hydrogen must be viewed as a donor of a fractional number of electrons  $\eta \leq 1$  electrons/atom to the d band. However, it should be noted that such a model is not a direct result of band calculations, since the magnetic properties are also affected by the change in the exchange interaction, which is not yet possible to include in the calculations; the large volume effects accompanying dissolution of hydrogen in Ni-Me alloys should also be kept in mind. The diversity of the magnetic properties of Ni-Me alloys make them convenient model objects for clarifying different aspects of the influence of hydrogen. Since the properties of hydrogen solutions in alloys also differ considerably, it makes sense to examine several Ni-Me-H systems systematically.

1) Ni-Fe-H system. Figure 12 shows the dependence  $\sigma_0(n)$  for  $\gamma$  solutions of hydrogen and nickel<sup>44</sup> and Ni-Fe alloys.<sup>50</sup> The  $\gamma_2$  phase of Ni-H solutions is paramagnetic for  $T \geq 4.2$  K and, in addition, in the temperature range  $T < 250$  K, the minimum solubility of hydrogen in this phase is  $n_{\gamma_2}^{min} = 0.7$ . Specimens with  $n < 0.7$  consist of a mixture of phases ( $\gamma_1 + \gamma_2$ ), while their magnetization is proportional to the content of the  $\gamma_1$  phase with  $\sigma_0(n_{\gamma_1}^{max}) \approx \sigma_0^{Ni}$  and decreases linearly with hydrogen concentration (curve 1 in Fig. 12). Stratification into  $\gamma_1$  and  $\gamma_2$  phases was not observed in solutions of hydrogen in Ni-Fe alloys with  $x_{Fe} \geq 0.1$ . As can be seen from Fig. 12, for alloys with 10, 20, and 40 at.% Fe, the spontaneous magnetization decreases with increasing  $n$  and, in addition, for  $n \leq 0.8$ , the dependences  $\sigma_0(n)$  are nearly linear, while for  $n > 0.8$ , a small but systematic deviation of  $\sigma_0$  toward higher values begins. The dependence  $\sigma_0(n)$  for the alloy with 60 at.% Fe is nearly linear up to  $n = 1$ . The behavior of  $\sigma_0$  of alloys with 66.1 and 67.5 at.% Fe is more complicated. For the alloy with 66.1 at.% Fe,  $\sigma_0$  depends little on the hydrogen concentration up to  $n \sim 0.5$  and then begins to decrease. For the alloy with 67.5 at.% Fe,  $\sigma_0$  increases with hydrogen concentration for small  $n$ , reaches a maximum value

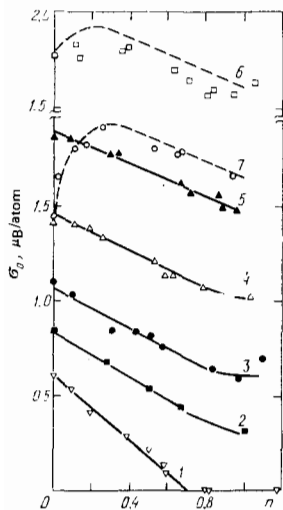


FIG. 12. The dependence of the spontaneous magnetization  $\sigma_0$  at  $T=0$  K and atmospheric pressure on the hydrogen content  $n$  in alloys Ni-Fe with different concentration of iron.<sup>50</sup> At.% Fe: 1) 0; 2) 10; 3) 20; 4) 40; 5) 60; 6) 66.1; 7) 67.5. The dashed line shows the dependence  $\sigma_0(n)$  for alloys with 66.1 and 67.5 at.% Fe, calculated using relation (4.3). The dimensions of  $\sigma_0$  are  $\mu_B/\text{atom}$  of the Ni-Fe alloy.

$\approx 1.85 \mu_B/\text{atom}$  at  $n \sim 0.3$ , and then decreases monotonically.

The first thing that draws attention in looking at the dependence  $\sigma_0(n)$  for alloys with  $x_{Fe} \leq 0.6$  is the presence of a linear section for  $n \leq 0.8$  and deviation from linearity for  $n > 0.8$ . We recall that a composition  $n \sim 0.7 - 0.8$  is singular for all  $\gamma$  hydrogen solutions in alloys based on nickel (and palladium) studied up to the present time: for  $n \geq 0$ , the nature of the dependences  $\Delta V_0(n)$  changes (see Fig. 9). The reasons for the appearance of these anomalies are not clear, so that it makes sense for the present to limit the discussion to magnetic properties of the solutions Ni-Fe-H with  $n \leq 0.8$ . The values of the slopes  $\partial\sigma_0/\partial n$ , obtained with a linear approximation to the experimental dependences  $\sigma_0(n)$  with  $n \leq 0.8$  for alloys containing 60 at.% Fe, decrease monotonically and approximately linearly in absolute magnitude, as the iron content in the Ni-Fe alloys increases (and, correspondingly, the electron concentration  $N^*$  of these alloys decreases), from  $\approx 0.6 \mu_B/\text{H atom}$  at  $x_{Fe} = 0.1$  to  $\approx 0.4 \mu_B/\text{H atom}$  at  $x_{Fe} = 0.6$ .

As we can see, the sign and order of magnitude of the effects observed agree with the value  $\partial\sigma_0^f/\partial n \approx -1 \mu_B/\text{H atom}$  predicted by the proton model (i.e., essentially the rigid band model), but, at the same time, the difference between the experimentally obtained values of  $\partial\sigma_0/\partial n$  and  $\partial\sigma_0^f/\partial n$  is still appreciable. It should be noted that as long as a ferromagnet remains strong (i.e., at  $T=0$  K, holes occur only in its  $d\uparrow$  subband),  $\sigma_0 \sim p\uparrow = p$ , the total number of holes in the  $d$  band, and is independent of the change in the exchange interaction and of the deformation of the bands, if it does not lead to a change in  $p$ . If, on the other hand, holes appear as a result of hydrogenation both in  $d\uparrow$  and in  $d\downarrow$  subbands, then in the rigid band approximation, this will cause a

decrease in  $\sigma_0$  with  $|\partial\sigma_0/\partial n| > |\partial\sigma_0^f/\partial n|$ , since the effect of pumping electrons from the  $d\uparrow$  to the  $d\downarrow$  subband will be added to the decrease in  $\sigma_0$  due to filling of the subband by hydrogen electrons. Thus, it is reasonable to ascribe the observed values of the slopes  $\partial\sigma_0/\partial n \sim -0.6 - 0.4 \mu_B/\text{H atom}$  to the change in the band structure of Ni-Fe-H solutions occurring with the penetration of hydrogen and accompanied by an increase in the number of holes  $p$  in the  $d$  band. The experimental values of  $\partial\sigma_0/\partial n$  can be explained within the scope of the rigid  $d$  band model by assuming that hydrogen is a donor of a fractional number of electrons  $n \sim 0.5$  electron/H atom in the  $d$  band of Ni-Fe alloys.

Let us go back to Fig. 12. It is evident from a comparison with Fig. 10 that for all Ni-Fe alloys with  $x_{Fe} \leq 0.675$  the concentration dependences of  $\sigma_0$  with the introduction of hydrogen into the alloys and with the substitution of iron by nickel are similar: for some concentration,  $\sigma_0$  reaches a maximum value  $\sigma_0^{\text{max}} \approx 1.86 - 1.9 \mu_B/\text{atom}$  and then begins to decrease. The similarity of the dependences  $\sigma_0(n)$  for alloys with 66.1 and 67.5 at.% Fe and the dependences  $\sigma_0(x_{Ni})$  in the Ni-Fe system is even more complete, which can be demonstrated as follows. For alloys with  $x_{Fe} \leq 0.6$ , the magnetization decreases linearly both with substitution of Fe by Ni and with an increase in the hydrogen concentration. Let us introduce, following Ref. 50, for each specific Ni-Fe alloy with  $x_{Fe} \leq 0.6$ , the coefficient  $\xi$ , relating the changes in the composition of Ni-Fe binary alloys and changes in  $n$ , leading to the same changes in  $\sigma_0$ :

$$\Delta x_{Fe} = \frac{(\partial\sigma_0/\partial n)}{(\partial\sigma_0/\partial x_{Fe})} n = -\xi n. \quad (4.3)$$

Equation (4.3) reflects the experimental fact that the dependence  $\sigma_0(n)$  for these alloys can be approximately obtained from  $\sigma_0(x_{Fe})$  by an appropriate change in scale along the concentration axis. Extrapolation of an approximately linear dependence  $\xi(x_{Fe})$  to alloys with  $x_{Fe} = 0.661$  and  $0.675$  gives  $\xi \approx 0.185$ . The dependences  $\sigma_0(n)$  for these alloys constructed with such a value of the rescaling coefficient  $\xi$  are shown in Fig. 12 by the dashed lines. It is evident that they agree with the experimental data.

An analogous correspondence occurs between the Curie points of Ni-Fe alloys and hydrogen solutions based on them.

In the  $\text{Ni}_{90}\text{Fe}_{10}$  alloy in an inert medium, the Curie point increases with pressure<sup>76</sup> with slope  $(dT_c/dP)_{\text{in}} \sim 0.5 \text{ K}\cdot\text{kbar}^{-1}$ . In a hydrogen atmosphere, the Curie point of this alloy decreases monotonically with pressure (see Fig. 5). A completely different pattern is observed for Invar Ni-Fe alloys.<sup>49,50</sup> The results of the determination of the dependence of the Curie point of the alloy with 67.5 at.% Fe on pressure in an inert medium and in hydrogen are presented in Fig. 13. It is evident that in an inert medium  $T_c$  of the alloy decreases linearly with slope  $(dT_c/dP)_{\text{in}} = -5.05 + 0.1 \text{ K}\cdot\text{kbar}^{-1}$  with pressures up to 20 kbar. In a number of papers (for example, in Ref. 76), it is shown that for Ni-Fe Invars the dependence  $T_c(P)$  in an inert medium

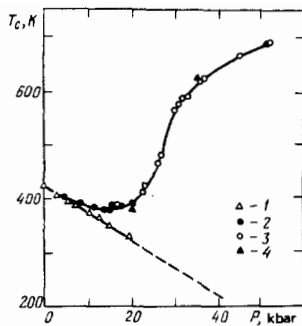


FIG. 13. The dependences of the Curie point of the  $\text{Fe}_{67.5}\text{Ni}_{32.5}$  alloy on pressure in an inert medium (1—data in Ref. 49) and in hydrogen (2—data in Ref. 49, 3—Ref. 50, 4—are the computed values; see subsection a in Sec. 2).

is nearly linear (dashed line in Fig. 13) at higher pressures as well.

An increase in the hydrogen concentration in the alloy with an increase in pressure leads to a deviation in the dependence  $T_c(P_{\text{H}_2})$  from that in an inert medium toward higher values of  $T_c$ . For  $P_{\text{H}_2} > 15$  kbar, the Curie points of  $\text{Ni}_{32.5}\text{Fe}_{67.5}\text{-H}$  solutions begin to increase, reaching  $\sim 700$  K at  $P_{\text{H}_2} = 50$  kbar. Table II presents the values of the hydrogen concentrations  $n$  on the curve of Curie points in the alloy with 67.5 at.% Fe at  $P_{\text{H}_2} = 20.35$  and 51 kbar. We note that the steepest dependence  $T_c(P_{\text{H}_2})$  of the  $\text{Ni}_{32.5}\text{Fe}_{67.5}\text{-H}$  solution is observed in the pressure range where the solubility of hydrogen in the alloy increases most rapidly ( $\sim 25\text{--}35$  kbar).

Assuming that the correspondence established by Eq. (4.3) between  $\sigma_0$  of alloys with and without hydrogen is also valid for  $T_c$  and  $(dT_c/dP)_{\text{in}}$ , it is possible to describe the dependence  $\Delta T_c^{\text{exp}}$ , namely, the difference between the values of  $T_c$  in hydrogen and in an inert medium under the same pressure. With this approach,  $\Delta T_c(P)$  will consist of

$$\Delta T_c^n = T_c(x_{\text{Fe}} - \xi n) - T_c(x_{\text{Fe}}), \quad (4.4)$$

related to the change in  $T_c$  without pressure due to the introduction of hydrogen into the alloy and

$$\Delta T_c^P = \left[ \left( \frac{dT_c(x_{\text{Fe}} - \xi n)}{dP} \right)_{\text{in}} - \left( \frac{dT_c(x_{\text{Fe}})}{dP} \right)_{\text{in}} \right] P, \quad (4.5)$$

arising due to the different pressure dependence of the Curie points of the alloys with and without hydrogen. Results of this calculation are presented in Table II and in Fig. 13. The  $T_c$  for the Ni-Fe alloys are taken from Ref. 72 and  $(dT_c/dP)_{\text{in}}$  from Ref. 77.

TABLE II. Parameters for Ni-Fe-H solutions.

$x_{\text{Fe}}$	$n$ *)	$P_{\text{H}_2}$ , kbar	$-\xi n$	$\Delta T_c^n$ , K	$\Delta T_c^P$ , K	$\Delta T_c^n + \Delta T_c^P$ , K	$\Delta T_c^{\text{exp}}$ , K
0.675	0.041	20	0.018	58	2	60	71
0.675	0.735	35	0.136	285	90	375	365
0.675	0.99	51	0.183	365	160	525	520
0.1	0.395	21.5	0.1	-115	-5	-120	-145

\*) The values of  $n$  with  $P_{\text{H}_2}$  from the third column and  $T = T_c(P_{\text{H}_2})$  are indicated.

As can be seen from Table II and Fig. 13, the computed values of  $\Delta T_c^n + \Delta T_c^P$  agree well with  $\Delta T_c^{\text{exp}}$ . We note that at high pressures the contribution of  $\Delta T_c^P$  to the sum  $\Delta T_c^n + \Delta T_c^P$  is not small and, thus, the agreement between the latter quantity and  $\Delta T_c^{\text{exp}}$  indicates the validity of (4.3) for describing the dependences of both  $T_c$  and  $(dT_c/dP)_{\text{in}}$  of the Ni-Fe Invars on their hydrogen content. Therefore, the correspondence (4.3) permits estimating the trend in the change of  $(dT_c(n)/dP)_{\text{in}}$ , which would be very difficult to do experimentally. The last line of Table II presents the results of an analogous calculation for a non-Invar alloy with 10 at.% Fe. It is evident that Eq. (4.3) satisfactorily describes the behavior of  $T_c(P_{\text{H}_2})$  for this alloy as well.

Thus, for the Ni-Fe alloys in the entire range of compositions studies  $0.1 \leq x_{\text{Fe}} \leq 0.675$  both the dependences  $\sigma_0(n)$  and  $\sigma_0(\Delta x_{\text{Fe}})$  as well as the dependences  $T_c(n)$  and  $T_c(\Delta x_{\text{Fe}})$  are similar and, in addition, they have the same similarity coefficients  $\xi$ . This can formally be represented as a similarity of the dependences  $\sigma_0$  and  $T_c$  on the electron concentration with hydrogenation and substitution of iron by nickel, respectively, and then the coefficients of such similarity  $\zeta = (Z_{\text{Ni}} - Z_{\text{Fe}}) \xi = 2\xi$  will give the effective number of electrons introduced by hydrogen into the conduction band of the metal. The presence of this similarity for Ni-Fe alloys with  $x_{\text{Fe}} > 0.6$ , which are weak collectivized ferromagnets (for which at  $T = 0$  K holes occur both in the  $d$  and  $d$  sub-band<sup>72</sup>), is strong evidence of the validity of the rigid band model for describing the magnetic properties of all fcc Ni-Fe alloys and the rigid d-band model for hydrogen solutions based on them. However, the number of electrons  $\zeta$  contributed by hydrogen to the d band, determined from the magnetic measurements, is only some effective phenomenological quantity. For this reason, the study of such properties for a number of different alloys is a necessary step in order to clarify the true role of the increase in the degree of filling of the d band by electrons in the change of the magnetic properties of hydrogen-saturated alloys.

2) Ni-Co-H system. Hydrogen solutions in fcc alloys  $\text{Ni}_{70}\text{Co}_{30}$  and  $\text{Ni}_{40}\text{Co}_{60}$ , which are strong collectivized ferromagnets, were studied in Ref. 60. Dissolution of hydrogen in these alloys, as in strong collectivized Ni-Fe ferromagnets with  $x_{\text{Fe}} \leq 0.6$ , decreases  $\sigma_0$  and  $T_c$ . The linear approximation to the experimental dependences  $\sigma_0(n)$  for  $n < 0.8$  for single phase solutions  $\text{Ni}_{70}\text{Co}_{30}\text{-H}$  and  $\text{Ni}_{40}\text{Co}_{60}\text{-H}$  gives the slopes  $\partial \sigma_0 / \partial n = -0.76$  and  $-0.71 \mu_B / \text{H atom}$ , which agrees with the predictions of the rigid d-band model. In attempting to describe the dependences  $\sigma_0(n)$  and  $T_c(n)$  for the Ni-Co alloys with the same coefficients of similarity  $\xi$ , introduced by a relation similar to (4.3), such good agreement is not obtained between the computed and experimental values of  $\Delta T_c$  as for the Ni-Fe alloys, but, the sign and order of magnitude of the effect turn out to be correct.

3) Ni-Mn-H system. The dependence  $\sigma_0(x_{\text{Mn}})$  of disordered fcc Ni-Mn alloys is nonmonotonic (see Fig. 10). For nickel ( $N^* = 10$  electrons/atom), the spontaneous magnetization  $\sigma_0^{\text{Ni}} \approx 0.616 \mu_B / \text{atom}$ ; as nickel is re-

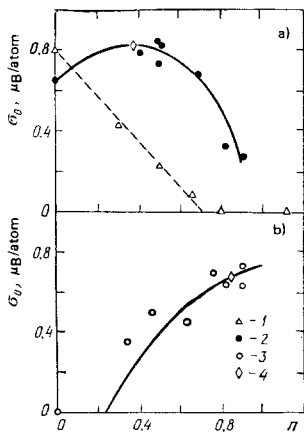


FIG. 14. The dependences of the spontaneous magnetization  $\sigma_0$  at  $T=0$  K on the hydrogen content  $n$  in disordered Ni-Mn alloys.<sup>75</sup> 1) 10; 2) 20; 3) 30 at.% Mn; 4) values of  $\sigma_0$ , used for calculating  $\zeta$ .

placed by manganese,  $\sigma_0$  increases and with  $x_{\text{Mn}} \approx 0.1$ , reaches the maximum value  $\sigma_0^{\text{max}} \approx 0.8 \mu_{\text{B}}/\text{atom}$  and then begins to decrease.<sup>68</sup> The Curie points decrease monotonically from 627 K for pure nickel to helium temperatures for the alloy with  $x_{\text{Mn}} \approx 0.26$ . The dependences  $\sigma_0(n)$ , obtained in Ref. 75 for hydrogen solutions in disordered Ni-Mn alloys with 10, 20, and 30 at.% Mn are presented in Fig. 14.

Stratification into  $\gamma_1$  and  $\gamma_2$  phases is observed in the  $\text{Ni}_{30}\text{Mn}_{10}\text{-H}$  system just as in the Ni-H system at atmospheric pressure and  $T \lesssim 150$  K. The  $\gamma_2$  phase is paramagnetic for  $T \geq 4.2$  K, while the approximately linear decrease in  $\sigma_0$  in the range of hydrogen concentrations  $0 \leq n \leq 0.7$  is due to the decrease in the content of the ferromagnetic  $\gamma_1$  phase in the two-phase mixtures ( $\gamma_1 + \gamma_2$ ) with increasing  $n$ .

The spontaneous magnetization of the  $\text{Ni}_{30}\text{Mn}_{20}\text{-H}$  solutions with increasing hydrogen concentration first increases, reaches the maximum value  $\sigma_0 \sim 0.8 \mu_{\text{B}}/\text{atom}$  at  $n \sim 0.37$  and then decreases. The Curie points at atmospheric pressure decrease monotonically from  $T_c = 354$  K at  $n=0$  to  $T_c \sim 100$  K at  $n=0.91$ .

The disordered alloy  $\text{Ni}_{70}\text{Mn}_{30}$  is paramagnetic for  $T \geq 4.2$  K. As can be seen from Fig. 14, injection of hydrogen into this alloy leads to the appearance of ferromagnetism. For  $n=0.9$ ,  $\sigma_0$  of the  $\text{Ni}_{70}\text{Mn}_{30}\text{-H}$  solution reaches values that are close to maximum in Ni-Mn alloys, while the Curie point rises to  $\sim 250$  K with  $n=0.85$ .

At temperatures close to room temperature, the behavior of the magnetization of the Ni-Mn-H solutions was also studied in Ref. 78 (for specimens that were electrolytically saturated with hydrogen at atmospheric pressure) and in Ref. 79 directly under high hydrogen pressure. The results of these papers agree with the data presented.

It is evident from a comparison of Figs. 14 and 10 that as for Ni-Fe and Ni-Co alloys, the dependences  $\sigma_0(n)$  and  $\sigma_0(\Delta x_{\text{Ni}})$  for the Ni-Mn alloys are qualitatively

similar. Let us introduce the coefficients  $\zeta = \Delta N^*/n$ , relating the changes in composition and, correspondingly, electron concentration  $N^*$  in the starting alloys with the changes in  $n$  leading to identical changes in  $\sigma_0$ . By comparing the values of  $\sigma_0(n)$  for the  $\text{Ni}_{80}\text{Mn}_{20}\text{-H}$  and  $\text{Ni}_{70}\text{Mn}_{30}\text{-H}$  solutions, indicated by the diamond-shaped symbols in Fig. 14, with the values of  $\sigma_0(x_{\text{Mn}})$  presented in Ref. 68 for Ni-Mn alloys, we obtain  $\zeta = 0.81$  and  $0.48$  electrons/H atom, respectively. The curves of  $\sigma_0(n)$  calculated for these values of  $\zeta$  for the  $\text{Ni}_{80}\text{Mn}_{20}$  and  $\text{Ni}_{70}\text{Mn}_{30}$  alloys are shown in Fig. 14 by the continuous lines. It is evident that they satisfactorily agree with the experimental dependences  $\sigma_0(n)$ .

Thus, the effect of dissolved hydrogen on  $\sigma_0$  of Ni-Mn alloys is completely analogous to the effect of substituting manganese by nickel. There is no such analogy for the Curie points for alloys with 10 and 20 at.% Mn: an increase in the nickel content in Ni-Mn alloys increases  $T_c$ , while injecting hydrogen decreases  $T_c$ . The dependences  $T_c(n)$  and  $T_c(x_{\text{Ni}})$  again become similar for alloys with 30 at.% Mn: when this alloy is saturated with hydrogen up to  $n=0.85$  (the value of  $\sigma_0$  for this composition of the solution is indicated by the diamond-shaped symbols in Fig. 13b), its Curie point increases monotonically to  $\sim 250$  K, while for the  $\text{Ni}_{83.5}\text{Mn}_{16.5}$  alloy (which has the same value of  $\sigma_0$ )  $T_c \approx 400$  K.<sup>80</sup>

4) Ni-Cr-H system. Summarizing the results presented in Secs. 1-3, we can say that the dependences  $\sigma_0(n)$  for  $\gamma$  solutions based on nickel alloys with iron, cobalt, and manganese are analogous to the corresponding dependences  $\sigma_0(x_{\text{Ni}})$  for the starting binary alloys. A similar analogy also exists for the Curie points, breaking down only for Ni-Mn alloys with 10 and 20 at.% Mn. A completely different behavior of magnetic properties was discovered in Ref. 81 in Ni-Cr alloys, containing  $\leq 7$  at.% Cr. Replacement of chromium by nickel in these alloys increases both  $\sigma_0$  (Fig. 10) and  $T_c$ ,<sup>80</sup> while electrolytic saturation with hydrogen decreases them.<sup>81</sup>

5) Discussion of properties of Ni-Me-H solutions. Earlier, we discussed in detail one limiting case: the case of hydrogen solutions in strong collectivized ferromagnets (Ni-Co, Ni-Fe with  $x_{\text{Fe}} \leq 0.6$ ), when the concentration dependence of the magnetic properties of the starting alloys was determined primarily by the degree to which the d band was filled and not by its deformation.

The other limiting case, when the band structure is strongly deformed with a change in the composition of the alloys, is realized, for example, for the Ni-Cr and Ni-V alloys. In these alloys, the perturbing potential introduced by the Cr and V atoms is high enough to shift the virtual  $d^{\uparrow}$  levels of the impurity atoms above the Fermi energy (see Fig. 11c). The electrons from these states flow into the conduction band, increasing the degree of filling of the d states of nickel, which decreases  $T_c$  and  $\sigma_0$ . When such alloys are hydrogenated, electrons contributed by the hydrogen atoms also will primarily fill the d band of nickel, in view of its high density of states at the Fermi level, decreasing  $T_c$  and  $\sigma_0$ .

It is this picture that is observed on saturation of Ni-Cr alloys with hydrogen.<sup>81</sup>

Thus, in both limiting cases, the band theory of ferromagnetism permits describing the observed dependences  $\sigma_0(n)$  and  $T_c(n)$  assuming that the increase in the degree of filling of the d band of the metal by electrons when the metal is hydrogenated has a dominating effect on the magnetic properties. The situation with alloys for which the dependences  $\sigma_0(N^e)$  deviate from a straight line with slope  $\partial\sigma_0/\partial N^e \approx -1 \mu_B/\text{electron}$  only when the impurity content is appreciable is more complicated. Such magnets include Ni-Fe alloys with  $x_{Fe} > 0.6$  and Ni-Mn alloys with  $x_{Mn} \geq 0.1$  (see Fig. 10). These collectivized ferromagnets are weaker, i.e., at  $T=0$  K, an appreciable number of holes exist in them both in the  $d\uparrow$  and  $d\downarrow$  subbands. The question as to the role played by the deformation of the band structure in the formation of the dependences  $\sigma_0(x_{Ni})$  of such alloys is controversial at the present time, especially for the Ni-Fe alloys, which in this range of concentrations have anomalous physical properties (Invar nature). Here, it is more likely that the opposite occurs: the observed analogy to the behavior of  $\sigma_0$  (and in most cases  $T_c$ ) with increasing nickel content and with hydrogenation indicates the fact that it is the degree of filling of the d band and not its deformation, over quite a wide range of compositions ( $\Delta N^e \leq \zeta n \leq 0.5$  electrons/atom) that primarily determines the magnetic properties of the starting alloys (without hydrogen). Indeed, let us assume that the deviations at values of  $N^e$ , smaller than some limiting value  $N_{lim}^e$ , from the straight line

$$\sigma_0(N^e) \approx \sigma_0^{Ni} + (N^e - N_{lim}^e) \mu_B, \quad (4.6)$$

which describes well the behavior of the spontaneous magnetization of strong collectivized ferromagnets with a fcc lattice, for Ni-Fe and Ni-Mn alloys are due to sharp (occurring in the range  $\Delta N^e \ll 0.5$  electrons/atom) and qualitatively different changes in the band structure. Experiments show that for both groups of alloys the influence of hydrogen on  $\sigma_0$  of alloys with  $N^e < N_{lim}^e$  is completely equivalent to the effect of increasing their electron concentration. This equivalence is especially clearly illustrated by the coincidence of the maximum values  $\sigma_0^{max}$  on the curves of  $\sigma_0(n)$  for the solutions  $Ni_{32.5}Fe_{67.5}-H$  (Fig. 12,  $\sigma_0^{max} \approx 1.85 \mu_B/\text{atom}$ ) and  $Ni_{80}Mn_{20}-H$  (Fig. 14a,  $\sigma_0^{max} \approx 0.8 \mu_B/\text{atom}$ ) with maximum values on the corresponding curves of  $\sigma_0(N^e)$  for the Ni-Fe and Ni-Mn alloys (Fig. 10). Therefore, the effect of hydrogen on the band structure of the Ni-Fe alloys is opposite to the effect of the substitution of nickel by iron, or in the case of the Ni-Mn alloys, of substitution of nickel by manganese, i.e., in accordance with the starting assumption, it is qualitatively different. But, this is too unlikely: all the experimental and theoretical data taken together show that hydrogen must deform the d band, formed by the transition metal atoms, weakly and only increases the degree of filling of the band by electrons.

Thus, the analysis of the effect of hydrogen on the magnetic properties of the Ni-Fe and Ni-Mn alloys leads to the conclusion that the deviation of the dependences of these alloys from (4.6) is due not to a sharp

change in the structure of the d bands or in the nature of the exchange interaction in the region of the "anomalous" behavior of the dependences  $\sigma_0(N^e)$ , but at the very least due to changes, gradually accumulating over wide ranges of concentrations of the order of the total content of iron and manganese in the alloys. It should be noted that the concentration dependence of these changes is much weaker in the case of nickel alloyed with iron, when it was necessary to have  $\Delta N^e = (Z_{Ni} - Z_{Fe})x_{Fe} \approx 2 \cdot 0.6 = 1.2$  electrons/atom in order that the dependence  $\sigma_0(N^e)$  first deviate from (4.6), than in the case of alloying with manganese, when  $\Delta N^e$  constitutes  $\approx 3 \cdot 0.1 = 0.3$  electrons/atom. Probably, the stronger deformation of the band structure of nickel when it is alloyed with manganese rather than iron is what leads to the fact that, in contrast to all the Ni-Fe alloys studied, for Ni-Mn alloys with 10 and 20 at.% Mn, an analogy is not observed in the change of the Curie points with composition and with saturation by hydrogen.

### c) $Fe_{65}(Ni_{1-x}Mn_x)_{35}-H$ solutions

The  $Fe_{65}(Ni_{1-x}Mn_x)_{35}$  (% by weight) solutions are a classical system, in which over a period of many years the problems of the competition between ferro- and antiferromagnetic ordering in fcc metals was studied. This system gave the rare possibility of observing systematically the effect of hydrogen on both types of magnetic ordering using the same group of objects.

The substitution of nickel by manganese in the  $Fe_{65}(Ni_{1-x}Mn_x)_{35}$  system decreases the Curie point from  $T_c = 467$  K for the  $Fe_{65}Ni_{35}$  alloy to helium temperatures for the alloy with  $\sim 10\%$  Mn. With a higher manganese content, antiferromagnetic ordering arises in the system and the Neel point increases monotonically to  $T_N = 442$  K for the  $Fe_{65}Mn_{35}$  alloy. Both ferro- and antiferromagnetically ordered alloys exhibit anomalous physical properties, characteristic of Invars (see Refs. 82 and 83).

The technology that we developed for compressing hydrogen up to 70 kbar permitted obtaining  $\gamma$  solutions with compositions up to  $n \sim 1$  for alloys in the entire range of concentrations from  $Fe_{65}Ni_{35}$  to  $Fe_{65}Mn_{35}$ .<sup>84</sup> The dependences  $\sigma_0(n)$  and  $T_c(n)$  for the Fe-Ni-Mn-H solutions are presented in Fig. 15. The following is observed when the  $Fe_{65}(Ni_{1-x}Mn_x)_{35}$  alloys are saturated with hydrogen. The Neel points of the antiferromagnetic alloys decrease; ferromagnetic ordering arises at a definite hydrogen concentration  $n_f$ ; and, then, the Curie points of the ferromagnetic solutions increase monotonically. Therefore, the change in the magnetic properties of the  $Fe_{65}(Ni_{1-x}Mn_x)_{35}$  alloys with hydrogenation is analogous to their change with substitution of manganese by nickel (which increases the electron concentration  $N^e$ ). As shown in Ref. 85, when the  $Fe_{65}Ni_{31}Mn_3$  (atomic percent) alloy is saturated with hydrogen, the shape of its Mössbauer spectrum also approaches the shape of the spectrum for the  $Fe_{65}Ni_{35}$  alloy.

Let us introduce the similarity coefficients  $\zeta$  for the dependences of the magnetic properties of the alloys with and without hydrogen. If it is assumed that both

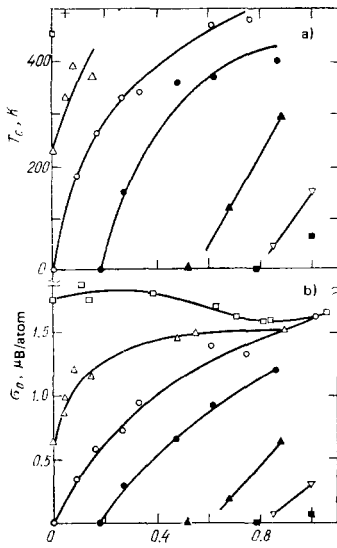


FIG. 15. The dependences  $\sigma_0(x)$  and  $T_c(x)$  for hydrogen solutions in fcc  $\text{Fe}_{65}(\text{Ni}_{1-x}\text{Mn}_x)_{35}$  alloys.<sup>84</sup> Notation as in Fig. 16.

the concentration dependence of the magnetic properties of the pseudobinary  $\text{Fe}_{65}(\text{Ni}_{1-x}\text{Mn}_x)_{35}$  system and the dependence of these properties on the hydrogen content in the alloys is determined primarily by the change in the degree of filling of the d band, then there must exist a common, for all these alloys and hydrogen solutions based on them, effective electron concentration  $N_f^e$  at which ferromagnetic ordering arises. Assuming that the quantities  $\zeta$  differ little for the alloys studied, from the equality

$$N^e + \langle \zeta \rangle n_f = N_f^e,$$

using the values of  $N^e$  and  $n_f$  presented in Table III, by the method of least squares we obtain  $\langle \zeta \rangle = 0.7$  electrons/H atom and  $N_f^e = 8.35$  electrons/atom. The quantities  $N_f^e - N^e$  and  $\zeta = (N_f^e - N^e)/n_f$  are also presented in Table III. It is evident that the sign and order of magnitude of the  $\zeta$  obtained in this manner agree with the assumption that the degree of filling of the d band plays a dominant role in the formation of the composition dependences of the magnetic properties of alloys studied with respect to nickel and hydrogen.

The results of investigations of hydrogen solutions in  $\text{Fe}_{65}(\text{Ni}_{1-x}\text{Mn}_x)_{35}$  alloys not only confirm the previously developed views on the nature of the influence of hydrogen on the magnetic properties of transition metals but

TABLE III. Parameters for hydrogen solutions in  $\text{Fe}_{65}(\text{Ni}_{1-x}\text{Mn}_x)_{35}$  alloys

Wt.% Mn	$T_c$ , K	$T_N$ , K	$N^e$ , Electron/atom	$N_f^e - N^e$ , Electron/atom	$n_f$	$\zeta$ , Electron/atom
0	467	—	8.68	-0.33	—	—
4.5	228	—	8.54	-0.19	—	—
10	—	—	8.38	-0.03	0	—
17	—	160	8.17	0.18	0.18	1.00
24	—	253	7.97	0.38	0.58	0.66
29	—	431	7.82	0.53	0.81	0.65
35	—	442	7.62	0.70	0.94	0.74

$\zeta = (N_f^e - N^e)/n_f$ ;  $N_f^e = 8.35$  electrons/atom in the Fe-Ni-Mn alloy.

also permit clarifying new aspects of this influence. The point is that the magnetic properties of the  $\text{Fe}_{65}(\text{Ni}_{1-x}\text{Mn}_x)_{35}$  alloys<sup>82,83</sup> and hydrogen solutions based on them<sup>84</sup> are described well by the equations of the theory of very weak collectivized ferromagnetism.<sup>86,87</sup> From these equations, in particular, it follows that for weak collectivized ferromagnets

$$\frac{T_c}{\sigma_0} = \frac{1}{2\pi k_B \mathcal{N}(\epsilon_F)} \left[ \frac{3\nu_1^2 - \nu_2}{\nu_1^2 - \nu_2} \right]^{1/2}, \quad (4.7)$$

where  $k_B$  is Boltzmann's constant,  $\mathcal{N}(\epsilon_F)$  is the density of states at the paramagnetic Fermi level  $\epsilon_F$ , while  $\nu_m = \mathcal{N}^{(m)}(\epsilon_F)/\mathcal{N}(\epsilon_F)$ . In fcc ferromagnets, the Fermi level occurs near the maximum of the density of states  $\mathcal{N}(\epsilon)$ ,<sup>68</sup> which leads to  $\nu_2 \leq 0$ . For  $\nu_2 \leq 0$ , the values of the factors in Eq. (4.7) enclosed by the square brackets depend weakly on the magnitudes of the parameters entering into it, varying from 3 at  $\nu_2 = 0$  to 1 for  $\nu_2 \rightarrow -\infty$ . In the case of a parabolic band, this factor equals 2. Thus, knowing  $T_c$  and  $\sigma_0$ , for a weak collectivized ferromagnet, it is possible to estimate as well the density of states at the paramagnetic Fermi level

$$\frac{T_c}{\sigma_0} \approx 1/\sqrt{2} \cdot \pi k_B \mathcal{N}(\epsilon_F). \quad (4.8)$$

The dependence  $T_c(\sigma_0)$  for the  $\text{Fe}_{65}(\text{Ni}_{1-x}\text{Mn}_x)_{35}$  system is shown in Fig. 16. It is evident that the values of  $T_c$  of the specimens studied as a function of  $\sigma_0$  lie approximately on a single curve (in order to show how strongly the dependences  $T_c(\sigma_0)$  can deviate from one another for different collectivized ferromagnets, a point for nickel is indicated in Fig. 16 by the diamond-shaped symbol). It follows from Eq. (4.8) that the existence of a common dependence  $T_c(\sigma_0)$  for all Fe-Ni-Mn alloys and hydrogen solutions based on them is proof of a unique relation between the values of  $T_c$  and  $\sigma_0$  for these materials and  $\mathcal{N}(\epsilon_F)$  at the paramagnetic Fermi level.

This result correlates well with all the facts indicating a weak deformation of d bands and small changes in the dependences of the exchange interaction as a function of the degree of filling of the d band accompanying hydrogenation of fcc nickel alloys, including,

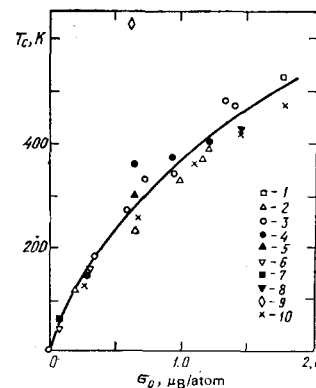


FIG. 16. Curie points  $T_c$  as a function of the spontaneous magnetization  $\sigma_0$  at  $T = 0$  K. 1-7)  $\gamma$  hydrogen solutions in  $\text{Fe}_{65}(\text{Ni}_{1-x}\text{Mn}_x)_{35}$  alloys<sup>51</sup> (1-0; 2-4.5; 3-10; 4-17; 5-24; 6-29; 7-35 wt.% Mn); 8) Ni-Fe alloys, containing 67.5 at.% Fe<sup>45,46</sup>; 9) nickel; 10)  $\text{Fe}_{65}(\text{Ni}_{1-x}\text{Mn}_x)_{35}$  alloys.<sup>82</sup>

the Ni-Fe Invars. Indeed, if the possibility of random coincidences is neglected, then in order that the weak collectivized ferromagnets with identical density of states  $\mathcal{N}(\varepsilon_F)$  at the paramagnetic Fermi level have equal Curie points and equal values of spontaneous magnetization over a wide range of values of  $\mathcal{N}(\varepsilon_F)$ , several conditions must be satisfied simultaneously: 1) the shape of the d bands of these ferromagnets must be the same; 2) the degree of filling of the d-bands must be the same; 3) the relative shift in the  $d\uparrow$  and  $d\downarrow$  sub-bands  $\Delta = I\sigma$  at all temperatures must be the same, i.e., the parameters  $I$  of the effective exchange interaction must be equal. Therefore, the results presented in Fig. 16 for the  $\text{Fe}_{65}(\text{Ni}_{1-x}\text{Mn}_x)_{35}$  alloys support the fact that when manganese is replaced by nickel in this pseudobinary system, as well as when the alloys are saturated with hydrogen, the change in the magnetic properties is due primarily to the increase in the degree of filling of the d band and, in addition, the phenomenological coefficients  $\zeta < 1$  electrons/H atom for the Fe-Ni-Mn-H solutions are close to the values  $\eta$  of the number of electrons contributed by the hydrogen atoms above the Fermi level.

These results explain to a certain extent one of the most complex problems arising in the discussion of the influence of hydrogen on the magnetic properties of transition metals, namely, the role of volume effects: the  $\text{Fe}_{65}(\text{Ni}_{1-x}\text{Mn}_x)_{35}$  alloys, just as the Ni-Fe alloys with  $x_{\text{Fe}} > 0.6$ , are Invars, whose characteristic feature is the strong dependence of the magnetic properties on volume.

The continuous line in Fig. 17 illustrates the dependence  $\sigma_0(N^0)$  for fcc Ni-Fe alloys at  $P=1$  bar. The dashed lines indicate the analogous dependences for  $P = -50$  and  $+50$  kbar, calculated assuming that the volume dependence of  $\sigma_0$  is linear using the experimental values of  $(1/\sigma_0)(\partial\sigma_0/\partial P)_{1n}$ , obtained under conditions of hydrostatic compression.<sup>47,77</sup> For  $N^0 \leq 9$  electrons/atom, the slope of the curve  $\sigma_0(N^0)$  for  $P = -50$  kbar increases sharply. For example, when  $N^0$  decreases from 8.9 to 8.7 electrons/atom,  $\sigma_0$  increases by  $\sim 0.9 \mu_B/\text{atom}$ . If the collectivized ferromagnet is strong [and the number of holes in the d bands of fcc alloys based on nickel is such that they must become strong

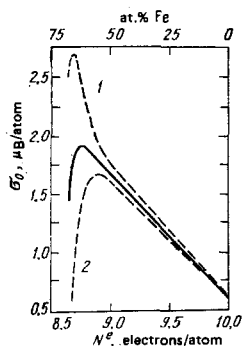


FIG. 17. Concentration dependences of  $\sigma_0$  for Ni-Fe alloys. Continuous curve is for  $P=1$  bar<sup>67, 68</sup>; 1) computed curve for  $P = -50$  kbar; 2) for  $P = +50$  kbar (see Sec. 3).

ferromagnets, when the magnetization reaches values  $\sigma_0(N^0) \sim \sigma_0^{N^0} + (N^0 - 10)\mu_B$ , a change in the degree of filling of the d band by  $\Delta N^0 = 8.9 - 8.7 = 0.2$  electrons/atom increases  $\sigma_0$  by only  $\sim 0.2 \mu_B/\text{atom}$ . The increase in  $\sigma_0$  by an additional amount  $\sim (0.9 - 0.2) = 0.7 \mu_B/\text{atom}$  can occur only as a result of an additional decrease in the number of electrons in the d band due to another mechanism, for example, by a transfer of  $\sim 0.7$  electrons/atom into the s band. The latter is unlikely, since this number of electrons is comparable to the total number of occupied states in the s band.

Thus, in order that the dependence  $\sigma_0(N^0)$  at  $P = -50$  kbar illustrated in Fig. 17 be realized, this pressure must lead to catastrophic changes in the band structure (and exchange interaction in Invar alloys. The dissolution of  $n \sim 1$  of hydrogen in such alloys causes an increase in the volume that is equivalent to the action of a negative pressure  $\sim 150$  kbar, and at the same time, as we have seen, it changes little the shape of the d band and the dependence of the exchange interaction parameter on the degree of filling of the band. We recall that when the Ni-Fe Invars with 66.1 and 67.5 at.% Fe are hydrogenated, their spontaneous magnetization does not increase above the value  $\sigma_0^{\text{max}} \sim 1.9 \mu_B/\text{atom}$ , maximum for Ni-Fe alloys without hydrogen (see Fig. 12). Since the compression of Invars leads to a strong decrease in  $\sigma_0$  (see Fig. 17, curve 2), this suggests that the dependence  $\sigma_0(V)$  relative to the volume  $V_0$  at  $P \sim 1$  bar is not symmetrical: for  $V < V_0$ , the magnetization increases with increasing  $V$  and for  $V \sim V_0$  reaches a stationary value and subsequently remains practically constant.

It is interesting that in contrast to the dependences  $\sigma_0(n)$ , the dependences  $T_c(n)$  for the Ni-Fe alloys studied can be explained by assuming that the main effect of the injection of hydrogen is in fact the increase in volume and by using the dependences  $T_c(V)$  obtained under conditions of compression (see Ref. 51). As shown in Ref. 88, the observed values of  $T_c(n)$  can also be explained by the dependence of the Curie points only on volume with saturation of the intermetallides Y-Fe and Ce-Fe by hydrogen. However, at least in the case of nickel alloys, the possibility of describing the dependences  $T_c(n)$  within the scope of the rigid d-band model with reasonable values of  $\eta$  and the unjustifiably high estimates for values of  $\sigma_0$  for hydrogen solutions in Invar alloys taking into account volume effects (using values of  $\partial\sigma_0/\partial V$  obtained under compression) cast doubt on the physical content of estimates of the effect of volume changes on the Curie point as well.

Summarizing the above presentation, it must be stated that the problem of the role of volume effects in the change of the magnetic properties of transition metals accompanying hydrogenation is nontrivial and is an interesting field for further research.

#### d) Applicability of the rigid d-band model for describing the magnetic properties of other Me-H solutions

1) *Hydrogen solutions in fcc alloys based on 3d metals.* The concept of hydrogen as a donor of a fractional

number of electrons in a weakly deformed d band of the metal-solvent, which is one of the most significant results of the study of magnetic properties of  $\gamma$  solutions Ni-Me-H makes it possible to predict at least qualitatively the behavior of these properties for a number of systems. For example, as  $n$  increases,  $\sigma_0$  and  $T_c$  of strong collectivized ferromagnets [Ni-Cu, Ni-Zn, Co-Fe; for Ni-Cu alloys, this is confirmed experimentally (see Ref. 89, 90, 51)] and of alloys for which  $\partial\sigma_0/\partial N^e > 0$  with a low impurity content (Ni-V, Co-N, Co-Cr), must decrease. As a result of the high density of states at the Fermi level of nickel and cobalt, the electrons of the dissolving hydrogen must fill the d band in the fcc alloys of these metals with nontransition elements (Ni-Al, Ni-Ge, Ni-Sb, and so on) as well, again decreasing  $\sigma_0$  and  $T_c$ . The increase of  $\sigma_0$  with increasing hydrogen concentration must, apparently, be observed only for those alloys with  $\partial\sigma_0/\partial N^e > 0$ , for which the dependences  $\sigma_0(N^e)$  deviate from (4.6) only for a large impurity content, i.e., it is to a large extent due to the degree of filling of the d band (Ni-Fe alloys with  $x_{Fe} > 0.6$ ; Ni-Mn with  $x_{Mn} > 0.1$ ).

2) *Hydrogen solutions in 3d metals with hcp lattice.* A necessary condition for the use of the rigid d-band model to describe magnetic properties of Me-H solutions is knowing how these properties depend on the degree of filling of the d-band in the starting materials (without hydrogen). In the case of fcc metals, such information can be obtained, for example, from the dependences  $\sigma_0(N^e)$  and  $T_c(N^e)$  for 3d metal alloys, closely positioned in Mendeleev's table, whose properties are described well by the rigid band model. The concentration dependences of magnetic properties with an hcp crystal lattice were studied in much less detail, primarily because of the relatively narrow intervals of the mutual solubility of 3d metals in hexagonal phases. However, for  $N^e \geq 7.7$  electrons/atom, these dependences for hcp and fcc alloys, apparently, are similar, which is the key for discussing the properties of  $\epsilon$  hydrogen solutions at least in iron ( $N^e = 8$  electrons/atom) and cobalt ( $N^e = 9$  electrons/atom).<sup>65</sup> Indeed, the values of  $\sigma_0$  of fcc alloys of 3d metals closely positioned in the periodic table lie along a single curve as a function of  $N^e$  (see Fig. 10). When  $N^e$  decreases to  $\approx 8.8$  electrons/atom,  $\sigma_0$  increases approximately linearly with slope  $\partial\sigma_0/\partial N^e \approx -1 \mu_B/\text{electron}$  (Ni-Cu, Ni-Co, and Ni-Fe alloys), reaches a maximum, and begins to decrease. For  $N^e \approx 8.35$  electrons/atom, the alloys become paramagnetic down to helium temperatures. Then antiferromagnetic ordering arises and the Neel point increases monotonically up to  $T_N \approx 440$  K at  $N^e = 7.65$  electrons/atom (Fe<sub>65</sub>(Ni<sub>1-x</sub>Mn<sub>x</sub>)<sub>35</sub> alloys). Available data on the magnetic properties of hcp metals and alloys fall into an analogous scheme. Hcp Fe-Mn alloys ( $N^e = 7.71-7.82$  electrons/atom) are antiferromagnets with Neel points  $\approx 230$  K.<sup>91</sup> Extrapolation from the Fe-Ru and Fe-Os alloys shows that at atmospheric pressure, the metastable hcp modification of iron ( $N^e = 8$  electrons/atom) must also be an antiferromagnet, but with a lower Neel point  $T_N \sim 100$  K.<sup>92</sup> Hcp cobalt ( $N^e = 9$  electrons/atom) is a ferromagnet with  $\sigma_0 = 1.72 \mu_B/\text{atom}$ .

Alloying cobalt with nickel ( $9 \leq N^e \leq 9.2$  electrons/atom) leads to an approximately linear decrease in  $\sigma_0$  with slope  $\partial\sigma_0/\partial N^e \approx -1 \mu_B/\text{electron}$ .<sup>93,94</sup>

Assuming that as in the case of fcc alloys, the dependence  $\sigma_0(N^e)$  for alloys with hcp lattice is determined over quite a wide range of concentrations primarily by changes in  $N^e$ , we shall now discuss the properties of  $\epsilon$  hydrides of cobalt and iron, described at the beginning of Sec. 4. Injection of hydrogen decreases  $\sigma_0$  of cobalt with initial slope  $\partial\sigma_0/\partial n|_{n=0} \approx -0.6 \mu_B/\text{H atom}$ , which, as can be seen from a comparison with the dependence  $\sigma_0(N^e)$  for hcp Co-Ni alloys, agrees with the predictions of the rigid d-band model. In the case that this model is valid for describing the magnetic properties of Fe-H solutions, an increase in hydrogen concentration in hcp iron must lead to (as observed, for example, with hydrogenation of fcc Fe-Ni-Mn alloys), a suppression of antiferromagnetic ordering the appearance of spontaneous magnetization at some value  $n = n_f$  and further to a monotonic increase in  $\sigma_0$  and  $T_c$ . The observed transformation of antiferromagnetic hcp iron into a ferromagnet with  $\sigma_0 \approx 2.2 \mu_B/\text{atom}$  and  $T_c \gg 80$  K with  $n \approx 0.8$  hydrogen dissolved in it qualitatively agrees with this dependence of magnetic properties on the hydrogen content.

For the Fe-H system, it is possible to introduce the coefficient  $\zeta = \Delta N^e/n$ , the "effective" number of electrons contributed by hydrogen to the d band of the metal, relating the changes in  $N^e$  and  $n$  that lead to an identical change in the magnetic properties of hcp iron. In analogy to the dependence  $\sigma_0(N^e)$  for fcc alloys, it may be expected that for  $8 < N^e < 9$  electrons/atom, the curve of  $\sigma_0(N^e)$  for hcp alloys also passes through a maximum. This means that for  $n \approx 0.8$ , the point  $\sigma_0(N_{Fe}^e + \zeta n) \approx 2.2 \mu_B/\text{atom}$  either falls on the continuation of the linear dependence  $\sigma_0(N^e)$  for Ni-Co alloys (with slope  $\varphi = \partial\sigma_0/\partial N^e \approx -1 \mu_B/\text{electron}$ ) or lies below this line. Therefore,

$$\sigma_0^h = [N_{Co}^e - (N_{Fe}^e + \zeta n)] \varphi \approx 2.2 \mu_B/\text{atom},$$

from where  $\zeta \approx 0.6$  electrons/atom, which is a reasonable estimate.

3) *Hydrogen solutions in tcc alloys of 4d metals.* In contrast to metals at the end of the 3rd series, 4d metals do not have properties that are simply and uniquely related to the degree of filling of the d band, which makes it difficult to study experimentally the problem of the status of hydrogen in solutions based on them. However, it can be stated that all available experimental data on the effect of hydrogen on the physical properties of these metals and their alloys (electron heat capacity, magnetic permeability, shape of the Mössbauer spectra, and so on) are uniquely explained if it is assumed that hydrogen is a donor contributing of the order of 1 electron/H atom to the weakly deformed conduction band of the metal-solvent. A detailed discussion of these problems and references to the original papers are given, for example, in Refs. 10, 14, 30, and 95. In this review, we would like to consider only the recently discovered,<sup>96</sup> quite unexpected appearance

of localized magnetic moments on ruthenium atoms on hydrogenation of Pd-Ru alloys (local moments for 4d metal atoms in a metallic matrix were not previously observed<sup>95</sup>) and its interpretation within the scope of the rigid d band model.

The experimental results are as follows. Measurements of the magnetic permeability and low-temperature heat capacity have shown that for the fcc Pd-Ru alloys studied, containing up to 4 at.% Ru (the decomposition of Pd-Ru solid solutions into  $\gamma + \epsilon$  phases prevents obtaining homogeneous alloys with a large ruthenium content), there are no local magnetic moments. When these alloys are saturated with hydrogen, there is an isomorphous phase transition  $\gamma_1 - \gamma_2$ , accompanied by an abrupt increase in the hydrogen concentration; the quantity  $n_{\gamma_2}^{\text{min}}$ , the minimum solubility of hydrogen in the  $\gamma_2$  phase, constitutes  $\approx 0.6$  at  $T = 100^\circ\text{C}$  for the Pd-H system and decreases to  $\approx 0.4$  for the Pd<sub>96</sub>Ru<sub>4</sub>-H system. In the Pd-Ru-H hydrides formed, ruthenium atoms already have local magnetic moments. The magnitude of these moments is maximum for  $n = n_{\gamma_2}^{\text{min}}$ ; further increase in the hydrogen concentration in the region of homogeneity of the  $\gamma_2$  phase causes them to decrease monotonically and then to vanish (at  $n \approx 0.8$ ).

The ranges of applicability of the rigid band model for describing the properties of 4d metal alloys are much narrower than for 3d metals.<sup>95,96</sup> For alloys of palladium with its nearest neighbors in Mendeleev's table, namely, silver and rhodium, it, apparently, works satisfactorily but already for alloys with the next left neighbor, ruthenium, it is qualitatively incorrect. From a comparison of the concentration dependences of the coefficient of electron heat capacity (proportional to the density of states at the Fermi level) when palladium is alloyed with silver and ruthenium, it may be concluded that the addition of even small (0.6 at.%) quantities of ruthenium shifts the Fermi level relative to the d band upward in energy with the magnitude of this shift corresponding to an average rate of filling of the d band of palladium  $\partial N^e / \partial x_{\text{Ru}} \approx 1.3$  electrons/Ru atom (we recall that if the rigid band model is valid, the addition of ruthenium into palladium must, on the contrary, lead to an emptying of the d band with  $\partial N^e / \partial x_{\text{Ru}} = Z_{\text{Ru}} - Z_{\text{Pd}} = -2$  electrons/Ru atom). Within the scope of Friedel's theory,<sup>71</sup> this means that the virtual bound d states of ruthenium atoms are appreciably above the Fermi level of palladium, and part of the electrons in these states flow into its conduction band.

Ruthenium atoms in Pd-Ru alloys do not have local magnetic moments. Therefore, the virtual d levels of these atoms are not split into sublevels with oppositely oriented spin (this situation is schematically illustrated in Fig. 18a), since the exchange energy of such splitting is less than the energy broadening of these levels due to hybridization with conduction band states. With the formation of  $\gamma_2$  hydrides, the virtual levels of ruthenium split (Fig. 18b) and due to the different degree of filling of the  $d\uparrow$  and  $d\downarrow$  sublevels, local magnetic moments appear on the ruthenium atoms. According to Refs. 95 and 96, the splitting could be due to a decrease in the energy broadening of the virtual levels of ruthen-

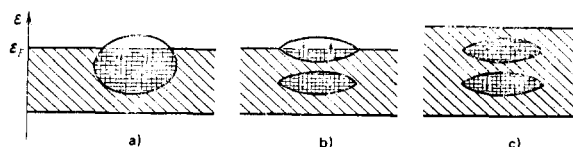


FIG. 18. Diagram illustrating the behavior of virtual bound states of ruthenium atoms in  $\gamma$  solutions Pd-Ru-H<sup>96</sup> a)  $n = 0$ ; b)  $n \gtrsim n_{\gamma_2}^{\text{min}}$ ; c)  $n \gtrsim 0.8 \gg n_{\gamma_2}^{\text{min}}$ .

ium atoms due to a decrease in the degree of their hybridization with the conduction band states of palladium with the formation of hydrides, since in this case the virtual levels are shifted into a region of energies with low density of states of palladium. This conclusion is based on the experimental fact that with the formation of the  $\gamma_2$  phase of Pd-Ru-H alloys, as measurements of the electron heat capacity have shown, the d band of palladium is entirely filled and the Fermi level, intersecting the d sublevels of ruthenium, falls into the range of energies where there are only states of the s type with low density. In view of the low density of states near the Fermi level, the increase in the hydrogen concentration (and, correspondingly, electron concentration) in the region of homogeneity of the  $\gamma_2$  phase of Pd-Ru-H solutions leads to a rapid increase in the Fermi energy. The virtual d states of ruthenium atoms are gradually filled, the magnitude of the uncompensated local moments decreases monotonically and, when the d sublevels are completely filled, the local moments disappear (Fig. 18c).

4) Ni-Fe-C solutions. As is evident from the discussion in Sec. 2, the rigid d-band approximation, in spite of its simplicity, is useful for explaining, and sometimes predicting as well, the properties of hydrogen solutions in a number of transition metals and their alloys. The available experimental data on the effect of carbon on the magnetic properties of Ni-Fe alloys<sup>97,98</sup> permit examining the problem of the applicability of this approximation and to describe the properties of substitution Me-C solutions, the nearest analog to Me-H solutions.

Figure 19 shows the change in  $\sigma_0$  of fcc Ni-Fe alloys

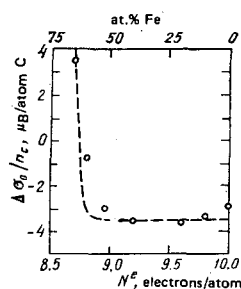


FIG. 19. The dependence of  $\Delta\sigma_0/n_c$  of the change in the spontaneous magnetization  $\sigma_0$  at  $T = 0$  K for carbon alloyed fcc Ni-Fe alloys as a function of the electron concentration of alloys  $N^e$ .<sup>97</sup>  $n_c$  is the atomic ratio carbon metal. The dashed line shows the computed curve for  $\xi_C = 3.5$  electrons/C atom (see subsection d in Sec. 4).

when carbon is injected into them with  $n_c \approx 0.01$ .<sup>97</sup> It is evident that for alloys containing up to  $\approx 55$  at. % Fe ( $N^e \approx 8.9$  electrons/atom), the dissolution of carbon decreases the spontaneous magnetization and, in addition, the value of  $\Delta\sigma_c/n_c$  depends weakly on the concentration of the Ni-Fe alloys and lies in the range  $-3$ – $-3.5 \mu_B/C$  atom. With a further increase in the iron content in the alloys, the values of  $\Delta\sigma_c/n_c$  increase rapidly and become positive  $x_{Fe} \approx 0.63$  ( $N^e \approx 8.74$  electrons/atom). From a comparison of the dependence  $\sigma_0(N^e)$  presented in Fig. 10 for Ni-Fe alloys, it is evident that the initial slope of the dependences  $\sigma_0(n_c)$  must depend precisely in this manner on the concentration of the Ni-Fe alloys, if the main effect of the injection of carbon atoms is related (as in the case of the injection of hydrogen atoms) to the increase in the degree of filling of the 3d band of the metal-solvent.

The value of the slope  $\Delta\sigma_0/n_c \approx -(3-3.5) \mu_B/\text{atom}$  for Ni-Fe alloys with  $x_{Fe} \leq 0.55$ , which are strong collectivized ferromagnets, is interesting. Carbon, in contrast to hydrogen, has four valence electrons and if the rigid band model (the cation model) were valid for describing solid Ni-Fe-C solutions, then the dissolution of carbon in these alloys would decrease the spontaneous magnetization with slope  $\partial\sigma_0^s/\partial n_c \approx -4 \mu_B/C$  atom. It is very probable that the observed difference between the experimental values of  $\Delta\sigma_0/n_c$  and  $\partial\sigma_0^s/\partial n_c$  is due to the fact that the valence states of carbon, just as the valence states of hydrogen, are strongly hybridized with the s states of the conduction band of the metal-solvent, decreasing their energy. Part of the electrons contributed by carbon atoms to the conduction band are used to fill the additional states arising in this manner below the Fermi energy and carbon is a donor of a fractional number of electrons  $\eta_c < 4$  electrons/C atom in the d band of the metal (we recall that in view of the high density of d states at the Fermi level of transition metals, practically all electrons with energy above  $\epsilon_F$  will fall into the d band).

In analogy to Me-H systems, we shall introduce the coefficient  $\zeta_c = \Delta N^e/n_c$ , the effective number of electrons contributed by carbon atoms to the d band of Ni-Fe alloys. Then, using the dependence  $\sigma_0(N^e)$  presented in Fig. 10 for the Ni-Fe alloys, it is possible to estimate in the rigid d-band approximation the values of  $(\Delta\sigma_0/n_c)_{\text{comp}} = [\sigma_0(N^e + \zeta_c n_c) - \sigma_0(N^e)]/n_c$  for the Ni-Fe-C solutions. The curve computed for  $\zeta_c = 3.5$  electrons/C atom and  $n_c = 0.01$  is shown in Fig. 19 by the dashed line and agrees satisfactorily with the experimental values of  $\Delta\sigma_0/n_c$  for all Ni-Fe-C solutions studied in Ref. 97.

Data available on the effect of carbon on the Curie point of Invar Ni-Fe alloys ( $x_{Fe} \geq 0.6$ ) are collected together in Ref. 98. Carbon, just as hydrogen, increases the Curie points of Invars. The experimental data have a large spread, but the order of magnitude of the effect agrees with the predictions of the rigid d-band model.

## 5. SUPERCONDUCTIVITY OF HYDROGEN SOLUTIONS IN PALLADIUM ALLOYS

After Skoskiewicz<sup>99</sup> discovered in 1972 that superconductivity exists in palladium hydride, so much attention

has been and continues to be devoted to the study of superconducting properties of hydrogen solutions in palladium and its alloys that it is now simply impossible not to discuss this subject in a review concerning the properties of transition metal hydrides. However, the discussion will be carried out on a completely different plane than in the preceding section examining the magnetic properties of Me-H solutions. The extensive experimental and theoretical material accumulated shows that the physical nature of the appearance of superconductivity in Pd-H and Pd-Me-H systems is very complicated and it is hardly possible to expect that in the near future a simple model will appear describing even the concentration dependences of their superconducting transition temperatures  $T_c$ , since in order to estimate  $T_c$  it is necessary to have a detailed knowledge of the electron and phonon spectra of the solution, while hydrogen strongly changes both. A detailed review and discussion of available data on the superconducting properties of Me-H solutions can be found in Refs. 8, 9, 100, and 101. We shall consider only the problem of the different nature of the structural instabilities in the experimentally obtained Me-H solutions, which, as the latest studies have shown, can play an important role in the appearance of superconductivity with anomalously high  $T_c$  at least in the case of hydrogenation of palladium alloys with previous metals.

Superconductivity arises in Pd-H solutions for  $n \geq 0.8$ .<sup>99</sup> Further increase in hydrogen content, as shown in a number of papers, leads to a monotonic increase in the superconducting transition temperature to  $T_c \approx 8.8$  K at  $n=1$  (in Fig. 20, this dependence is shown by the dashed line).<sup>100</sup> Even higher values of  $T_c$  of the order of 13–17 K were obtained by implanting hydrogen into palladium alloys with previous metals, copper, silver, and gold.<sup>102</sup> Both in the case of palladium and in these alloys, at a certain irradiation dose, the thin

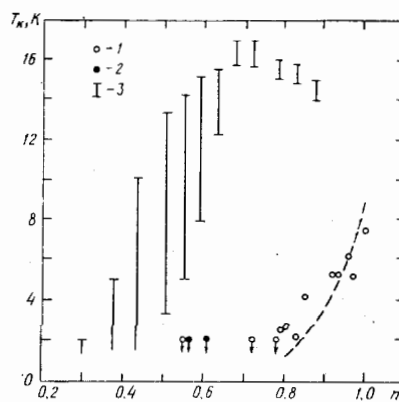


FIG. 20. Dependence of the superconducting transition temperature  $T_c$  on the atomic ratio hydrogen/metal  $n$ . 1) For solutions  $\text{Pd}_{80}\text{Ag}_{20}\text{-H}$ ;<sup>103</sup> 2)  $\text{Pd}_{60}\text{Cu}_{40}\text{-H}$ ;<sup>103</sup> (signs with arrows indicate that these specimens are not superconducting for  $T \geq 2$  K); 3)  $\text{Pd}_{65}\text{Cu}_{35}\text{-H}$ ;<sup>102</sup> (intervals are indicated in which the resistance of the specimens changes from 90 to 10% of the value of the residual resistance of the normal phase). Dashed curve shows the dependence  $T_c(n)$  for the Pd-H solutions.<sup>100</sup>

( $\sim 1500 \text{ \AA}$ ) hydrogen containing layer of the metal formed became superconducting and with further irradiation  $T_c$  increased, attained a maximum value  $T_c^m$  and began to decrease. In its turn, the dependence of  $T_c^m$  on the content of the alloying element in palladium for each of the binary systems Pd-Cu, Pd-Ag, and Pd-Au also had a maximum and, in addition, the maximum values of  $T_c^m$  constituted  $\approx 16.6$ ,  $15.6$ , and  $13.6 \text{ K}$ , respectively, for the  $\text{Pd}_{55}\text{Cu}_{45}$ ,  $\text{Pd}_{70}\text{Ag}_{30}$  and  $\text{Pd}_{84}\text{Au}_{16}$ . The typical dependence  $T_c(n)$  with hydrogen implantation in the  $\text{Pd}_{55}\text{Cu}_{45}$  alloy is presented in Fig. 20 (the accuracy of the estimates of the hydrogen concentration  $\delta n \sim 15\%$ ). The dependences  $T_c(n)$  for the  $\text{Pd}_{70}\text{Ag}_{30}$ -H and  $\text{Pd}_{84}\text{Au}_{16}$ -H solutions have an analogous character, only the value of the optimum hydrogen concentration at which the maximum value of  $T_c$  is attained changes ( $n_{\text{opt}} \approx 0.7, 0.8, \text{ and } 0.9$ , respectively, for alloys with Cu, Ag, and Au).

Using the technology for compressing hydrogen to high pressures, we were able to obtain macroscopic specimens of hydrides of palladium alloys with previous metals. It turned out that if for the Pd-H alloys, obtained by implantation, the value of  $T_c^m$  agrees well with the maximum values of  $T_c$  (with  $n \rightarrow 1$ ) for massive homogeneous specimens (see Ref. 100), then in the case of palladium-previous metal-hydrogen solutions, no such agreement is observed. The investigation of the  $\text{Pd}_{80}\text{Ag}_{20}$  and  $\text{Pd}_{60}\text{Cu}_{40}$  alloys (composition close to optimum for obtaining the maximum values of  $T_c$  with hydrogen implantation), saturated with hydrogen at  $P_{\text{H}_2} \leq 70 \text{ kbar}$ , showed<sup>103</sup> that the dependence  $T_c(n)$  for the solid  $\text{Pd}_{80}\text{Ag}_{20}$ -H solutions for  $n \leq 1$  is close to that for the Pd-H solutions, while in the  $\text{Pd}_{60}\text{Cu}_{40}$ -H system for  $n \leq 0.6$  and  $T \geq 2 \text{ K}$ , there is no superconductivity (see Fig. 20).

Thus our results show that the anomalously high values of  $T_c$  obtained with hydrogen implantation in palladium alloys with precious metals are due to the characteristics of the metastable states arising on implantation. It should be noted that at the present time there is no unified point of view as to how the alloying of palladium with previous metals should affect  $T_c$  in the case of the formation of hydrogen solutions based on the fcc lattice of the metal. For example, according to the theoretical estimates in Refs. 12 and 101, the superconducting transition temperature must in this case increase, while according to the theoretical estimates in Ref. 104 and estimates made in Ref. 105 based on an experimental study of the low-temperature heat capacity of nonsuperconducting solid  $\text{Pd}_{80}\text{Ag}_{20}$ -H solutions, it must decrease. The possibility that the instability of the crystal lattice (due to softening of some phonon modes and, therefore, increase in the electron-phonon interaction constant) can play an important role in obtaining high  $T_c$  with hydrogen implantation in palladium alloys with Cu, Ag, and Au was noted by Stritzker,<sup>102,100</sup> who discovered the interesting property that their  $T_c^m$  depend on the dose of implanted hydrogen  $\psi$ . For the Pd-Cu and Pd-Ag alloys with compositions close to optimum ( $T_c^m > 15 \text{ K}$ ), the monotonic increase in  $T_c$  with increasing  $\psi$  was sometimes replaced by its sudden de-

crease and vanishing of superconductivity for  $T > 1 \text{ K}$ , while the residual resistance  $R_{\text{res}}$  decreased discontinuously by  $10\text{--}20\%$ . Further increase in  $\psi$  led to a monotonic decrease in  $R_{\text{res}}$ , but the appearance of superconductivity for  $T > 1 \text{ K}$  was no longer observed. Stritzker explained this by the formation of a new non-superconducting phase with a smaller value of  $R_{\text{res}}$ .

Thus, the reason for the appearance of superconductivity with anomalously high values of  $T_c$  accompanying implantation of hydrogen into palladium alloys with precious metals is closely related precisely to the structural properties of these systems. We recall that the Me-H solutions based on transition metals in the VI-VIII groups studied had only either a fcc or a hcp metal sublattice. Since the palladium-precious metal alloys themselves already have a fcc structure, the structure of the hypothetical new phase, formed with implantation of hydrogen, must therefore differ from the previously observed structures. The study of the solid  $\text{Pd}_{60}\text{Cu}_{40}$ -H solutions, saturated with hydrogen at high pressure, has indeed led to the discovery of a new phase transition in them, accompanied by a tetragonal distortion of the fcc sublattice of the metal.<sup>106</sup>

The study of the isobars of the electrical resistance of the  $\text{Pd}_{60}\text{Cu}_{40}$  alloy in a hydrogen atmosphere in the pressure range of  $5\text{--}10 \text{ kbar}$  showed that with heating above  $T^* \sim 220^\circ \text{C}$  an irreversible phase transition occurs in the specimens and, in addition, the resistance decreases strongly in the transition process. This transition proceeds very slowly: even at  $T = 350^\circ \text{C}$ , the drift in the resistance continues for tens of hours. An x-ray diffraction analysis established that the metallic sublattice of  $\text{Pd}_{60}\text{Cu}_{40}$ -H specimens, obtained by holding at  $T = 200^\circ \text{C} < T^*$ ,  $5 \leq P_{\text{H}_2} \leq 20 \text{ kbar}$  and having the composition  $n \leq 0.47$ , retains fcc symmetry and, in addition, the value of  $\Delta V_0$  of the abrupt change in the unit-cell volume of the  $\text{Pd}_{60}\text{Cu}_{40}$  alloy accompanying hydrogenation agrees satisfactorily with the dependence  $\Delta V_0(n)$  presented in Ref. 52 (see Fig. 9) for  $\gamma$  hydrogen solutions based on palladium and its alloys. The diffraction pattern for these specimens has, however, some special features: lines of the  $\{111\}$  type are sharp, while the remaining lines are appreciably broadened, which can be interpreted as the result of the appearance of packing defects in the close-packed planes<sup>107</sup> or small tetragonal or orthorhombic distortion of the fcc sublattice.

$\text{Pd}_{60}\text{Cu}_{40}$ -H specimens, obtained by holding at  $250 \leq T \leq 350^\circ \text{C}$  (i.e., with  $T > T^*$ ) and  $P_{\text{H}_2} \leq 20 \text{ kbar}$ , had a metallic sublattice, whose symmetry can be described based on a fcc subcell (in what follows, the  $\gamma^1$  phase) with the axial ratio  $0.94 \leq c/a \leq 0.97$ . The hydrogen content in these specimens fell into the range  $0.3 \leq n \leq 0.5$ ; the volume per metal atom had approximately the same magnitude as for  $\gamma$  solutions  $\text{Pd}_{60}\text{Cu}_{40}$ -H with nearly the same values of  $n$ .

The study of  $\gamma^1$  specimens during annealing, which caused separation of hydrogen, led to some interesting results. When hydrogen is partially liberated after annealing at room temperature and atmospheric pres-

sure, the metal lattice remained tetragonal, while the quantity  $c/a$ , as a rule, decreased. The alloy retained the tetragonal structure even after annealing for six hours in a vacuum at 300 °C, which led to complete liberation of hydrogen, while the volume per metal atom decreased and assumed a value close to that for the starting Pd<sub>60</sub>Cu<sub>40</sub> alloy. With further annealing for several hours at  $T \geq 350$  °C, the structure of the alloy returned to the starting cubic structure. The return to the fcc structure occurred also after plastic deformation of the specimen at room temperature. These results show that at atmospheric pressure and  $T \geq 20$  °C, the  $\gamma^1$  structure of the Pd<sub>60</sub>Cu<sub>40</sub> alloy is not in thermodynamic equilibrium. At the same time, the metastability of this structure after complete liberation of hydrogen and even some increase in its degree of tetragonality support the proposition that the observed tetragonal distortions are mainly related not to the possible phase transitions in the hydrogen sublattice (for example, its ordering), but to a restructuring of the metal sublattice itself occurring in the Pd<sub>60</sub>Cu<sub>40</sub>-H solution.

One of the possibilities of such restructuring is atomic ordering. The presence of wide regions with ordered positioning of atoms in  $T$ - $c$  diagrams is characteristic both of the Cu-Pd system and a number of related systems. In particular, ordering in the region of compositions close to Cu<sub>3</sub>Pd leads precisely to tetragonal distortion of the fcc lattice of Cu-Pd alloys.<sup>108-110</sup> With ordering of this type, in addition to the main (structural) lines of the fcc lattice superstructural lines appear whose position is close to that for reflections from planes with mixed indices. For  $\gamma^1$  specimens, in addition to the main lines, 11 very weak and broad lines were observed and mixed indices could be assigned to all of them.

Thus, the results of the x-ray diffraction analysis permit asserting with quite a high degree of reliability that the formation of the  $\gamma^1$  phase in the Pd<sub>60</sub>Cu<sub>40</sub>-H system is accompanied by ordering of the metallic sublattice (even though an incomplete one, which is indicated by the large width of the superstructural lines compared to the width of the main lines). The appearance of packing defects in the close-packed planes of the metallic sublattice of the  $\gamma$  phase, formed at a lower temperature (which is manifested in the broadening of all lines except {111}), is apparently an intermediate stage of this process.

Thus, a new phase transition has been discovered in Pd<sub>60</sub>Cu<sub>40</sub>-H solutions, which does not have any analogs to previously studied hydrogen solutions based on group VI-VIII transition metals and their alloys. At the same time, it is still difficult to give a clear answer to the question as to whether or not the  $\gamma'$  phase arising at high pressure is the nonsuperconducting phase which sometimes forms on implantation of hydrogen and whose existence according to Ref. 102 in principle can explain the anomalously high values of  $T_c$ . However, it is possible to present some arguments supporting a positive answer. The formation of the  $\gamma'$  phase, just as the formation of the nonsuperconducting phase accompanying implantation, is accompanied by a decrease in

the electrical resistance. Strong local overheating in the process of implanting hydrogen and the high concentration of defects in the hydrogen containing layer produced create favorable conditions for occurrence of diffusion processes. We should also mention Ref. 101, wherein the possible relation of the values of the concentrations of the Pd-Cu, Pd-Ag, and Pd-Au alloys, for which maximum  $T_c$  were observed with hydrogen implantation, to the more favorable compositions for possible ordering of alloys without hydrogen is pointed out.

It should be noted that at the present time most superconducting Pd-Me-H solutions are synthesized by implantation. The study of hydrogen solutions in palladium alloys with precious metals has demonstrated the necessity of including the possibility of the existence of a structural instability in the physical description of the results obtained with specimens synthesized by this specific method. A vivid example, illustrating the need to take into account also the effect of radiation defects, was the discovery of superconductivity in pure Pd after irradiation by helium ions.<sup>111</sup>

Experiments were performed on palladium films with thicknesses up to 400 Å, grown out of the vapor phase on substrates (SiO<sub>2</sub>, Al<sub>2</sub>O<sub>3</sub>, Si), with temperature varying from 4.2 to 300 K. The energy of the He<sup>+</sup> ions was chosen to be quite high (130 keV), so that they would definitely pass through the palladium film and not be retained by it. The temperature of the film during irradiation did not exceed 8 K. At a definite irradiation dose,  $\psi \sim 10^{16}$  He<sup>+</sup> ions/cm<sup>2</sup>, palladium became superconducting, and the superconducting transition temperature rapidly increased and reached a value  $\approx 3.2$  K. Stritzker<sup>111</sup> interpreted the observed effect as the result of the suppression of spin fluctuations in palladium due to a decrease in the density of states at the Fermi level caused by the diffuseness of the Fermi surface resulting from the appearance of a large number of radiation defects.

It is interesting that a necessary condition for the appearance of superconductivity on irradiation of palladium by helium atoms is the preliminary presence of defects in the crystal structure, arising on the deposition of palladium on a cold substrate. In particular, irradiation of specimens in which these defects were annealed at 500 K generally did not lead to the appearance of superconductivity for  $T \geq 0.1$  K and, in addition, during the irradiation process, the residual resistance of such specimens increased, while for the unannealed specimens, it decreased. The increase in  $R_{res}$  during annealing is a normal phenomenon, since in this case the number of scattering centers increases. The decrease in the residual resistance of unannealed palladium films indicated, in this manner, the annealing of previously present defects formed during growth of these films on a cold substrate occurring with irradiation. The appearance of superconductivity only in unannealed specimens was, apparently, due to the fact that these defects, themselves annealing during irradiation, created favorable conditions for formation of specific radiation defects. As far as the radiation de-

facts that lead to the appearance of superconductivity are concerned, they could be palladium atoms in interstitial positions or even entire clusters of such atoms: x-ray measurements showed that irradiation by helium ions caused a strong increase in the crystal lattice constant of palladium of up to 0.4%, which corresponded to the presence of ~2% interstitial atoms.<sup>111</sup>

## 6. CONCLUSIONS

Working in the area of high-pressure physics, we are glad to note that the first results of application of high-pressure methods for obtaining hydrides of transition metals and studying their properties are already interesting and informative. This inspires confidence that a further development of this research, an increase in the pressure range and the range of objects and properties studied will lead to the discovery of many more new and unusual phenomena and will provide a deeper understanding of the physical nature of hydrides.

We thank V. L. Ginzburg for his interest in our work and for the suggestion that we write this review, E. G. Maksimov for valuable suggestions improving the paper, as well as S. N. Stishov, R. Z. Levitin, V. A. Somenkov, N. I. Kulikov, and B. K. Ponomarev for reading the manuscript and for valuable remarks.

- <sup>1</sup>T. Greham, Proc. Roy. Soc. **16**, 422 (1868); Phil. Mag. **36**, 63 (1868); C. R. Acad. Sci. **66**, 1014 (1868); Ann. Chim. Phys. (Paris) **14**, 315 (1868).
- <sup>2</sup>J. R. Lacher, Proc. Roy. Soc. A **161**, 525 (1937).
- <sup>3</sup>T. D. Lee and C. N. Yang, Phys. Rev. **87**, 410 (1952).
- <sup>4</sup>L. D. Landau and E. M. Lifshitz, *Statisticheskaya Fizika*, Nauka, Moscow (1976) [Engl. transl. *Statistical Physics*, Pergamon Press, New York, (1979)].
- <sup>5</sup>V. A. Somenkov, Ber. Bunsenges, Phys. Chem. **76**, 733 (1972).
- <sup>6</sup>Yu. Kagan and M. I. Klinger, J. Phys. C **7**, 2791 (1974).
- <sup>7</sup>A. M. Stoneham, Ber. Bunsenges. Phys. Chem. **76**, 816 (1972).
- <sup>8</sup>S. V. Vonsovskii, Yu. A. Izyumov, and E. Z. Kurmaev, *Sverkhprovodimost' perekhodnykh metallov, ikh splavov i soedinenii* (Superconductivity of Transition Metals, Their Alloys and Compounds), Nauka, Moscow (1977).
- <sup>9</sup>E. G. Maksimov and O. A. Pankratov, Usp. Fiz. Nauk **116**, 385 (1975) [Sov. Phys. Usp. **18**, 481 (1975)].
- <sup>10</sup>A. C. Switendick, Solid State Commun. **8**, 1463 (1970); Ber. Bunsenges. Phys. Chem. **76**, 535 (1972); *Hydrogen in Metals*, Ed. by G. Alefeld and J. Völkl, in: *Topics in Applied Physics*, Springer-Verlag, New York (1978), Vol. 28, p. 101.
- <sup>11</sup>D. A. Papaconstantopoulos and B. M. Klein, Phys. Rev. Lett. **35**, 110 (1975); D. A. Papaconstantopoulos, B. M. Klein, J. S. Faulkner, and L. L. Boyer, Phys. Rev. B **18**, 2784 (1978).
- <sup>12</sup>D. A. Papaconstantopoulos, B. M. Klein, E. N. Economou, and L. L. Boyer, Phys. Rev. B **17**, 141 (1978); D. A. Papaconstantopoulos, E. N. Economou, B. M. Klein, and L. L. Boyer in: Proc. Intern. Conf. on Hydrogen in Metals, Münster (1979), p. 733.
- <sup>13</sup>M. Gupta and A. J. Freeman, Phys. Rev. B **17**, 3029 (1978).
- <sup>14</sup>N. I. Kulikov, V. N. Borzunov, and A. D. Zvonkov, Phys. Status Solidi B **86**, 83 (1978); N. I. Kulikov, *ibid.* **91**, 753 (1979).
- <sup>15</sup>N. A. Galktionov, *Vodorod v metallakh* (Hydrogen in Metals), Metallurgiya, Moscow (1967).
- <sup>16</sup>P. V. Gel'd and R. A. Ryabov, *Vodorod v metallakh i splavakh* (Hydrogen in Metals and Alloys), Metallurgiya, Moscow (1974).
- <sup>17</sup>M. M. Antonov, *Svoistva gidridov metallov* (Properties of Metal Hydrides), Naukova Dumka, Kiev (1975).
- <sup>18</sup>S. A. Shavely and D. A. Vaughan, J. Am. Chem. Soc. **71**, 313 (1949).
- <sup>19</sup>B. Baranowski and M. Smialowski, J. Phys. Chem. Sol. **12**, 206 (1959).
- <sup>20</sup>V. Kh. Alimov, A. E. Gorodetskiĭ, A. P. Zakharov, and V. M. Sharapov, Dokl. Akad. Nauk SSSR **241**, 595 (1978).
- <sup>21</sup>S. A. Semiletov, R. V. Baranova, Yu. P. Khodyrev, and R. M. Imamov, Kristallografiya **25**, 1162 (1980) [Sov. Phys. Crystallogr. **25**, 665 (1980)].
- <sup>22</sup>B. Baranowski and R. Wiśniewski, Bull. Acad. Polon. Sci. Ser. Sci. Chim. **14**, 273 (1966).
- <sup>23</sup>R. Wiśniewski in: III Krajowa Narada Techniki Wysokich Ciśnień, Warszawa (1969), p. 62.
- <sup>24</sup>B. Baranowski and W. Bujnowski, Roczniki Chem. **44**, 2271 (1970).
- <sup>25</sup>M. Krukowski and B. Baranowski, J. Less-Common Met., **49**, 385 (1976).
- <sup>26</sup>B. Baranowski, cited in Ref. 10, Vol. 29, p. 157.
- <sup>27</sup>B. Baranowski, Zs. Phys. Chem. **114**, 59 (1979).
- <sup>28</sup>I. T. Belash and E. G. Ponyatovskii, Inventor's Certificate No. 741105 (USSR); Byul. Izobret. No. 22, 223 (1980).
- <sup>29</sup>V. E. Antonov, I. T. Belash, and E. G. Ponyatovskii in: *Fizika i tekhnika vysokikh davlenii* (High-Pressure Physics and Technology), Naukova Dumka, Kiev (1982), Vol. 9.
- <sup>30</sup>W. Wicke and H. Brodowsky, cited in Ref. 10, Vol. 29, p. 73.
- <sup>31</sup>V. E. Antonov, I. T. Belash, E. G. Ponyatovskii, and V. I. Rashchupkin, Fiz. Met. Metalloved. **48**, 75 (1979) [Phys. Met. Metallogr. (USSR)].
- <sup>32</sup>V. E. Antonov, I. T. Belash, and E. G. Ponyatovskii, Dokl. Akad. Nauk SSSR **223**, 1114 (1977).
- <sup>33</sup>V. I. Spitsyn, V. E. Antonov, O. A. Balakhovskii, I. T. Belash, E. G. Ponyatovskii, V. I. Rashchupkin, and V. Sh. Shekhtman, *ibid.* **260**, 132 (1981).
- <sup>34</sup>M. Krukowski and B. Baranowski, Roczniki Chem. **49**, 1183 (1975).
- <sup>35</sup>E. G. Ponyatovskii and I. T. Belash, Dokl. Akad. Nauk SSSR **224**, 607 (1975).
- <sup>36</sup>V. I. Spitsyn, E. G. Ponyatovskii, V. I. Antonov, I. T. Belash, and O. A. Balakhovskii, *ibid.* **247**, 1420 (1979).
- <sup>37</sup>V. E. Antonov, I. T. Belash, V. F. Degtyareva, E. G. Ponyatovskii, and V. I. Sheryaev, *ibid.* **252**, 1384 (1980) [Sov. Phys. Dokl. **25**, 490 (1980)].
- <sup>38</sup>V. E. Antonov, I. T. Belash, V. F. Degtyareva, and E. G. Ponyatovskii *ibid.* **239**, 342 (1978).
- <sup>39</sup>B. Baranowski and K. Bojarski, Roczniki Chem. **46**, 525 (1972).
- <sup>40</sup>I. T. Belash, V. E. Antonov, and E. G. Ponyatovskii, Dokl. Akad. Nauk SSSR **235**, 379 (1977).
- <sup>41</sup>V. E. Antonov, I. T. Belash, and E. G. Ponyatovskii *ibid.* **248**, 635 (1979).
- <sup>42</sup>E. G. Ponyatovskii, and I. T. Belash, *ibid.* **229**, 1171 (1976).
- <sup>43</sup>T. Greham, Phil. Trans. Roy. Soc. **156**, 415 (1866).
- <sup>44</sup>V. G. Tissen, V. E. Antonov, I. T. Belash, B. K. Ponomarev, and E. G. Ponyatovskii, Dokl. Akad. Nauk SSSR **242**, 1340 (1978).
- <sup>45</sup>B. Baranowski and K. Bochenska, Roczniki Chem. **38**, 1419 (1964).
- <sup>46</sup>B. Baranowski and S. Filipek, *ibid.* **47**, 2165 (1975).
- <sup>47</sup>D. Bloch, Ann. de Phys. **1**, 3 (1966).

- <sup>48</sup>E. G. Ponyatovskii, V. E. Antonov, and I. T. Belash, Dokl. Akad. Nauk SSSR **230**, 649 (1976).
- <sup>49</sup>E. G. Ponyatovskii, V. E. Antonov, and I. T. Belash, Fiz. Tver. Tela **18**, 3661 (1976) [Sov. Phys. Solid State **18**, 2131 (1976)].
- <sup>50</sup>V. E. Antonov, I. T. Belash, V. F. Degtyareva, B. K. Ponomarev, E. G. Ponyatovskii, and V. G. Tissen, *ibid.* **20**, 2680 (1978) [Sov. Phys. Solid State **20**, 1548 (1978)].
- <sup>51</sup>V. E. Antonov, I. T. Belash, E. G. Ponyatovskii, and V. G. Tissen in: Fizika i tekhnika vysokikh davlenii [High-Pressure Physics and Technology], Naukova Dumka, Kiev (1981), Vol. 9, p. 3.
- <sup>52</sup>B. Baranowski, S. Majchrzak, and T. B. Flanagan, J. Phys. F: Metal Phys. **1**, 258 (1971).
- <sup>53</sup>I. T. Belash, V. E. Antonov, and E. G. Ponyatovskii, Dokl. Akad. Nauk SSSR **235**, 128 (1977).
- <sup>54</sup>T. Schober and H. Wenzl, cited in Ref. 10, Vol. 29, p. 11.
- <sup>55</sup>I. S. Anderson, C. J. Carlile, and D. K. Ross, J. Phys. C **11**, L381 (1978).
- <sup>56</sup>O. Blaschke, R. Klemencic, P. Weinzierl, and O. J. Eder, Solid State Commun. **27**, 1149 (1978).
- <sup>57</sup>T. E. Ellis, C. B. Satterthwaite, M. H. Mueller, and T. O. Brun, cited in Ref. 12, p. 79.
- <sup>58</sup>I. T. Belash, B. K. Ponomarev, V. G. Tissen, N. S. Afonikova, V. Sh. Shekhtman, and E. G. Ponyatovskii, Fiz. Tver. Tela **20**, 422 (1978) [Sov. Phys. Solid State **20**, 244 (1978)].
- <sup>59</sup>E. O. Wollan, J. W. Cable, and W. C. Koehler, J. Phys. Chem. Solids **24**, 1141 (1963).
- <sup>60</sup>V. E. Antonov, I. T. Belash, B. K. Ponomarev, E. G. Ponyatovskii, and V. G. Thiessen, Phys. Status Solidi A **57**, 75 (1980).
- <sup>61</sup>R. Andrievskii and Ya. Umanskiĭ, Fazy vnedreniya (Interstitial Phases), Nauka, Moscow (1977).
- <sup>62</sup>W. E. Wallace, Ber. Bunsenges, Phys. Chem. **76**, 832 (1972).
- <sup>63</sup>M. Hanson, H. R. Khan, A. Knödler, Ch. J. Raub, J. Less-Common Met. **43**, 93 (1975).
- <sup>64</sup>H. R. Khan and Ch. J. Raub, *ibid.* **49**, 399 (1976).
- <sup>65</sup>V. E. Antonov, I. T. Belash, E. G. Ponyatovskii, V. G. Thiessen, and V. I. Shiryaev, Phys. Status Solidi A **65**, K43 (1981).
- <sup>66</sup>V. G. Thiessen, V. E. Antonov, I. T. Belash, V. K. Ponomarev, and E. G. Ponyatovskii, *ibid.* **48**, K185 (1978).
- <sup>67</sup>J. Crangle and G. C. Hallam, Proc. Roy. Soc. **272**, 119 (1963).
- <sup>68</sup>S. V. Vonsovskii, Magnetizm (Magnetism), Nauka, Moscow (1971).
- <sup>69</sup>M. J. Besnus, Y. Gottehrer, and G. Munsch, Phys. Status Solidi B **49**, 597 (1972).
- <sup>70</sup>B. K. Ponomarev and V. G. Tissen, Zh. Eksp. Teor. Fiz. **73**, 332 (1977) [Sov. Phys. JETP **46**, 173 (1977)].
- <sup>71</sup>J. Friedel, J. Phys. et Rad. **19**, 573 (1958); *ibid.* **23**, 692 (1962); Nuovo Cimento Suppl. **7**, 287 (1958).
- <sup>72</sup>G. T. Dubovka, Phys. Status Solidi A **24**, 375 (1974).
- <sup>73</sup>J. D. Fast, Vzaimodeistvie metallov s gazami (Interaction of Metals and Gases), Metallurgizdat, Moscow (1975), Vol. 2.
- <sup>74</sup>J. Friedel, Ber. Bunsenges. Phys. Chem. **76**, 828 (1972).
- <sup>75</sup>V. E. Antonov, I. T. Belash, and V. G. Thiessen, Phys. Status Solidi A **59**, 673 (1980).
- <sup>76</sup>J. M. Leger, C. Loriers-Susse, and V. G. Vodar, Phys. Rev. B **6**, 4250 (1972).
- <sup>77</sup>G. T. Dubovka and E. G. Ponyatovskii, Dokl. Akad. Nauk SSSR **206**, 83 (1972).
- <sup>78</sup>H. J. Schenk and H. J. Bauer, cited in Ref. 12, p. 350.
- <sup>79</sup>H. J. Schenk, H. J. Bauer, and B. Baranowski, Phys. Status Solidi A **52**, 195 (1979).
- <sup>80</sup>M. Khansen and K. Anderko, Struktura dvoynykh splavov (Structure of Binary Alloys), Metallurgizdat, Moscow (1962).
- <sup>81</sup>G. J. Zimmerman and H. J. Bauer, Zs. Phys. **229**, 154 (1969).
- <sup>82</sup>B. K. Ponomarev and S. V. Aleksandrovich, Zh. Eksp. Teor. Fiz. **67**, 1965 (1974) [Sov. Phys. JETP **40**, 976 (1974)].
- <sup>83</sup>G. T. Dubovka, E. G. Ponyatovskii, I. Ya. Georgieva, and V. E. Antonov, Phys. Status Solidi A **32**, 301 (1975).
- <sup>84</sup>V. E. Antonov, I. T. Belash, B. K. Ponomarev, E. G. Ponyatovskii, and V. G. Thiessen, *ibid.* **52**, 703 (1979).
- <sup>85</sup>T. Sohmura and F. E. Fujita, Solid State Commun. **25**, 43 (1978).
- <sup>86</sup>D. M. Edwards and E. P. Wohlfarth, Proc. Roy. Soc. A **303**, 127 (1968).
- <sup>87</sup>E. P. Wohlfarth, J. Appl. Phys. **39**, 1061 (1968).
- <sup>88</sup>K. H. J. Buschow, Solid State Commun. **19**, 421 (1976).
- <sup>89</sup>H. J. Bauer, G. Berninger, and G. Zimmermann, Zs. Naturforsch. **23a**, 2023 (1968).
- <sup>90</sup>H. J. Bauer, Zs. Angew. Phys. **26**, 87 (1968).
- <sup>91</sup>H. Ohno and M. Mekata, J. Phys. Soc. Jpn. **31**, 102 (1971).
- <sup>92</sup>H. Ohno, *ibid.* **31**, 92 (1971).
- <sup>93</sup>P. Weiss and R. Forrer, Ann. de Phys. **12**, 279 (1929).
- <sup>94</sup>R. M. Bozorth, Ferromagnetism, D. Van Nostrand, New York (1951), p. 279.
- <sup>95</sup>E. Wicke, J. Less-Common Met. **74**, 185 (1980).
- <sup>96</sup>K. Frolich, H. G. Severin, R. Hempelmann, and E. Wicke, Zs. Phys. Chem. N. F. **119**, 33 (1980).
- <sup>97</sup>M. C. Cadeville, R. Caudron, and C. Lerner, J. Phys. F **4**, L87 (1974).
- <sup>98</sup>M. C. Cadeville and E. P. Wohlfarth, Phys. Status Solidi A **26**, K157 (1974).
- <sup>99</sup>T. Skośkiewicz, *ibid.* **11**, K123 (1972).
- <sup>100</sup>B. Stritzker and H. Wühl, cited in Ref. 10, Vol. 29, 243.
- <sup>101</sup>B. N. Ganguly, Zs. Phys. B **22**, 127 (1975).
- <sup>102</sup>B. Stritzker, Zs. Phys. **268**, 261 (1974).
- <sup>103</sup>V. E. Antonov, I. T. Belash, E. G. Ponyatovskii, and V. I. Rashchupkin, Pis'ma Zh. Eksp. Teor. Fiz. **31**, 422 (1980)].
- <sup>104</sup>K. H. Benneman and J. W. Garland, Zs. Phys. **260**, 367 (1973).
- <sup>105</sup>G. Wolf, J. Yanke, and K. Bohmhammel, Phys. Status Solidi A **36**, K125 (1976).
- <sup>106</sup>V. G. Degtyareva, V. E. Antonov, I. T. Belash, and E. G. Ponyatovskii, *ibid.* **66**, 77 (1981).
- <sup>107</sup>A. Guinier, Théorie et technique de la radiocristallographie, Dunod, Paris (1956).
- <sup>108</sup>W. B. Pearson, A Handbook of Lattice Spacings and Structure of Metals and Alloys in: International Series of Monographs on Metal Physics and Physical Metallurgy, Ed. by G. V. Raynor, Pergamon Press, London (1964), Vol. 4.
- <sup>109</sup>K. Schubert, B. Kiefer, M. Wilkens, and R. Haufler, Zs. Metallkunde. **46**, 692 (1955).
- <sup>110</sup>D. M. Jones and E. A. Owen, Proc. Roy. Soc. B **67**, 297 (1954).
- <sup>111</sup>B. Stritzker, Phys. Rev. Lett. **42**, 1769 (1979).
- <sup>112</sup>B. Baranowski and K. Bojarski, Roczniki Chem. **46**, 1403 (1972).
- <sup>113</sup>V. E. Antonov, I. T. Belash, V. M. Kolytgin, and E. G. Ponyatovskii, Dokl. Akad. Nauk SSSR **248**, 131 (1979).
- <sup>114</sup>S. Majchrzak, Bull. Acad. Polon. Sci. Ser. Sci. Chim. **15**, 485 (1967).

Translated by M. E. Alferieff